Hydrological Processes

WILEY

RESEARCH ARTICLE OPEN ACCESS

Assessing Streamflow Responses to Future Climate and Land Use and Land Cover Change in a Transitional Brazilian Basin Between Semiarid Dry Forest and Humid Tropical Forest Biomes

Vanine Elane Menezes de Farias[1,2] | Suzana Maria Gico Lima Montenegro[2] | Richarde Marques da Silva[3] | Yunqing Xuan[1] | Bruno e Silva Ursulino[4] | Celso Augusto Guimarães Santos[5,6]

[1]Department of Civil Engineering, Faculty of Science and Engineering, Swansea University, Bay Campus, Swansea, UK | [2]Department of Civil and Environmental Engineering, Federal University of Pernambuco, Recife, Brazil | [3]Department of Geosciences, Federal University of Paraíba, João Pessoa, Paraíba, Brazil | [4]Department of Natural Resources, Federal Institute of Education, Science and Technology of Ceará - IFCE, Aracati, Ceará, Brazil | [5]Department of Civil and Environmental Engineering, Federal University of Paraíba, João Pessoa, Paraíba, Brazil | [6]Stokes School of Marine and Environmental Sciences, University of South Alabama, Mobile, Alabama, USA

Correspondence: Yunqing Xuan (y.xuan@swansea.ac.uk) | Celso Augusto Guimarães Santos (celso@ct.ufpb.br)

Received: 11 August 2025 | **Revised:** 25 October 2025 | **Accepted:** 27 October 2025

Funding: This study was partially financed by the Coordination for the Improvement of Higher Education Personnel (Coordenação de Aperfeiçoamento de Pessoal de Nível Superior—CAPES)—Code 001, and by the National Council for Scientific and Technological Development (Conselho Nacional de Desenvolvimento Científico e Tecnológico—CNPq). Support was provided through the INCT—National Water Security and Adaptive Management Observatory (406919/2022-4) under Call No. 58/2022/CNPq, and through research projects CNPq/MCTIC/BRICS 29/2017 (442335/2017-2), Universal MCTIC/CNPq 28/2018 (431980/2018-7) and Productivity in Research Scholarships—PQ (313392/2020-0, 313358/2021-4 and 309330/2021-1).

Keywords: climate variability | future projections | land use and land cover change | Northeast Brazil

ABSTRACT

Historically, severe drought events, coupled with land use and land cover changes, have significantly influenced streamflow behaviour This study enhances the understanding of these hydrological processes by assessing streamflow responses to future climate and land use and land cover change in a transitional Brazilian basin between semiarid and humid tropical forest biomes. Projections from 10 global climate models available through the Climate Change Dataset for Brazil (CLIMBra) were utilised incorporating bias correction via the Quantile Mapping method. Future land use and land cover changes were simulated using the land change modeller (LCM), while hydrological projections were generated through the soil and water assessment tool (SWAT), which was calibrated and validated with satisfactory performance, achieving coefficients of determination (R^2) and Nash-Sutcliffe (NSE) efficiencies in the ranges of 0.62–0.79 and 0.61–0.76 for calibration and 0.48–0.90 and 0.41–0.84 for validation, respectively. The results indicate a substantial expansion of agricultural and pasture areas, with a 280% increase over recent decades. Climate projections under the SSP2–4.5 and SSP5–8.5 scenarios show a progressive temperature rise and declining rainfall trends, with the SSP5–8.5 scenario exhibiting a steeper increase in temperature. Paradoxically, hydrological modelling suggests an intensification of streamflow extremes, with peak discharges ranging from 200 to 300 m^3/s, particularly, in regions prone to extreme precipitation events. Notably, under SSP5–8.5, a more pronounced rise in flood peaks is observed, indicating elevated flood risks, even in moderate emissions scenarios. These findings underscore the necessity for adaptive water resource management strategies to mitigate future hydrological vulnerabilities in the basin.

1 | Introduction

Changes in temperature, precipitation and land use and land cover have direct effects on streamflow regimes at watershed scales, leading to regional modifications in the hydrological cycle (Tenagashaw et al. 2022; Xue et al. 2022; Jiménez-Navarro et al. 2021). Historical data indicate that water resources are heavily impacted by these changes, triggering extreme events such as recurring droughts or floods (Xue et al. 2022). The hydrological cycle behaviour in the ecotone region between the Caatinga and Atlantic Forest biomes, located in Northeast Brazil and known as the 'Agreste', is of particular importance. This region is recognised as an internationally significant biodiversity hotspot (Santos et al. 2021). Furthermore, the 'Agreste' is critical for supplying water to major coastal cities in Northeast Brazil, such as the Capibaribe River basin, which provides water to the Metropolitan Region of Recife (MRR) (Aguiar et al. 2024). The MRR is one of the most climate-vulnerable regions in Brazil, being the first to declare a state of climate emergency and set a goal for carbon neutrality by 2050 (Leão et al. 2021). In this context, studying the impacts of temperature, precipitation and land use and land cover is essential for assessing the effects of climate change on the region's hydrological processes.

The Capibaribe River basin is a significant region in the state of Pernambuco, located in the transitional zone between the Caatinga and Atlantic Forest biomes. This basin plays a critical role in irrigation and public water supply, with much of the local population dependent on its water resources for agriculture and daily use. As a result, the region is, particularly, vulnerable to climate variability, including extreme events such as floods and droughts (Lima et al. 2018). Originating in the semiarid region, where the vegetation and climatic characteristics of the Caatinga biome predominate, the area is subject to periodic droughts (Silva et al. 2024). The basin extends to the coastal region, where the vegetation and environmental conditions transition to those typical of the Atlantic Forest biome.

In recent years, several studies have examined the effects of climate change on water resources in Brazil (Araujo et al. 2024; de Farias et al. 2024; Ballarin et al. 2023; Oliveira et al. 2023; Medeiros et al. 2022; Ribeiro Neto et al. 2014) as well as globally (Song et al. 2021; Almazroui et al. 2021; Wen et al. 2021; Todaro et al. 2022; Xue et al. 2022). However, studies analysing streamflow responses to land cover changes in ecotone regions—transitional zones between distinct biomes—remain limited both globally and in the specific context of Northeast Brazil, particularly, in the Caatinga–Atlantic Forest transition zone (Santos et al. 2021; Andrade et al. 2021).

Studies in Northeast Brazil suggest that future climate change scenarios could lead to an approximately 22% reduction in precipitation (de Andrade Costa et al. 2024). However, according to the IPCC (2023), the frequency and intensity of extreme climate events are expected to increase due to climate change, greenhouse gas emissions, carbon sequestration and deforestation. This paradox arises because the decline in total precipitation volume is accompanied by a greater concentration of rainfall over shorter periods, increasing the likelihood of intense precipitation events. At the same time, droughts and dry periods become more prolonged, failing to compensate for these short-lived, high-intensity rainfall episodes. These severe climatic changes will disproportionately impact regions with limited adaptive capacity. Therefore, it is essential to assess how these projections will affect land cover in the Caatinga–Atlantic Forest ecotone and develop appropriate response strategies.

Modelling catchment responses to climate forcing is inherently complex due to the wide range of climate-sensitive factors that must be considered (Almagro et al. 2017). Typically, such predictions involve coupling global climate models (GCMs) with other models to account for land use and land cover and hydrological processes. In this study, we followed the approach used by Silva et al. (2022), integrating GCMs with hydrological and land use and land cover models to evaluate the impact of climate change and land use and land cover on streamflow in the Capibaribe River basin. This region, located within the transitional zone between the Caatinga and Atlantic Forest biomes, presents unique ecological and climatic conditions, adding further complexity to the analysis.

While the overall goal is to assess these impacts, this study specifically seeks to advance the understanding of hydrological processes in complex transitional basins by addressing the following key research questions: (a) How do the projected dynamics of climate change and land use and land cover interact to impact streamflow regimes within a complex ecotone, where semiarid (Caatinga) and humid (Atlantic Forest) climate characteristics coexist?; (b) To what extent does the projected shift in precipitation patterns, specifically a potential decline in total rainfall coupled with more intense, concentrated events—alter hydrological extremes and key water balance components? and (c) How do distinct land cover typologies differentially mediate key hydrological processes, such as surface runoff and groundwater recharge, under future climate and LULC pressures?

2 | Materials and Methods

2.1 | Study Area

Located in the state of Pernambuco, Brazil (Figure 1), the Capibaribe River basin covers an area of approximately 7454 km^2. The region experiences a semiarid climate, with an average annual rainfall of 1300 mm and an average air temperature of 26°C (Ribeiro Neto et al. 2014). This region has faced extreme events, including periods of drought and flooding, which have resulted in numerous social, economic and environmental impacts. Structural interventions have been necessary to mitigate the effects of floods in the area (de Arruda Gomes et al. 2021).

The Capibaribe River basin is home to a population of 1.71 million people and supplies 36% of the water to the MRR (Ribeiro Neto et al. 2014). The basin exhibits a wide range of landscape features, resulting in diverse characteristics such as vegetation cover, precipitation patterns, topography, climate and soil types, which vary significantly across its length (da Silva et al. 2016). The eastern portion of the basin is dominated by native

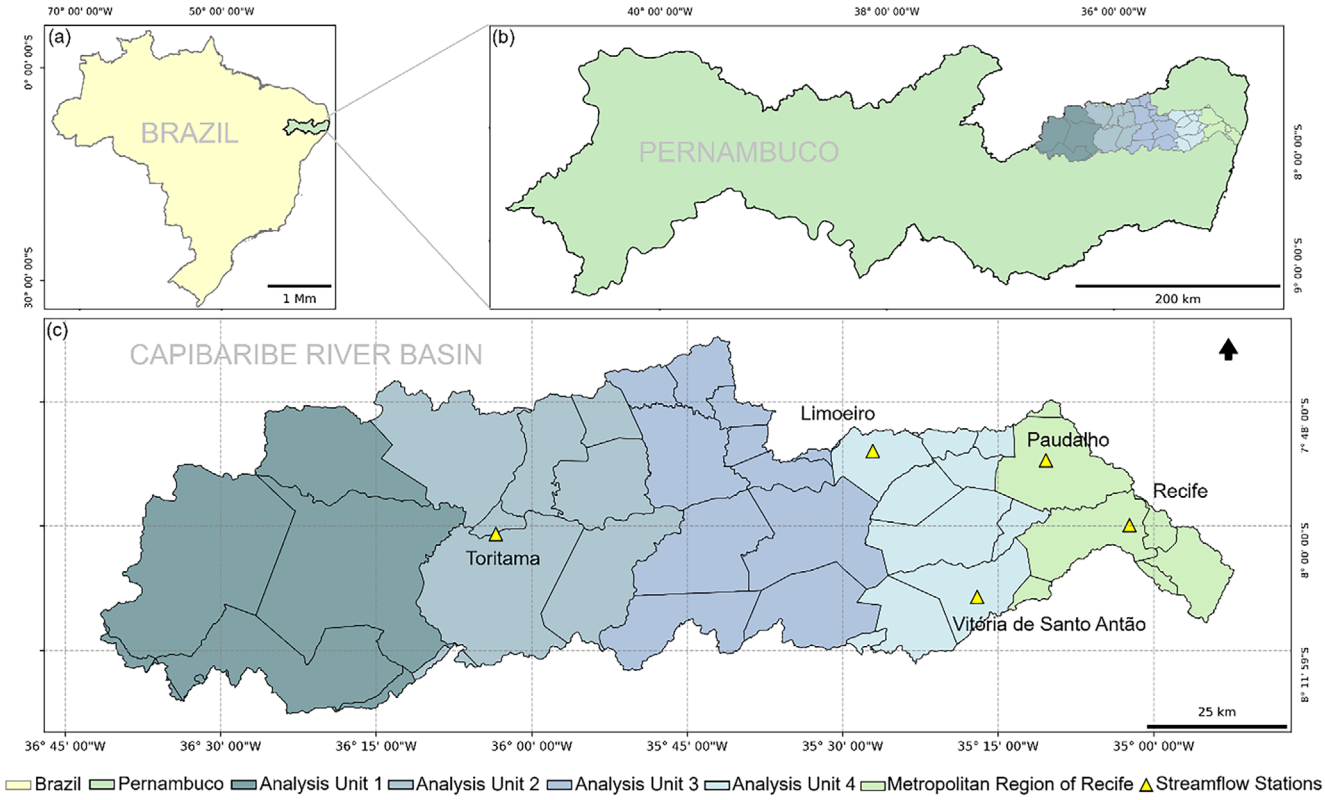

FIGURE 1 | Location of the Capibaribe River Basin study area. The panels illustrate: (a) the location of Pernambuco State within Brazil; (b) the position of the basin within Pernambuco and (c) a detailed view of the basin, its analysis units and the corresponding streamflow stations.

Atlantic Forest vegetation, while the western portion, within the Caatinga biome, is characterised by xerophytic vegetation (Santos et al. 2021). In addition, the basin includes urban areas, extensive monocultures of sugarcane and mosaics combining natural and anthropogenic elements, including large pasture areas (Alves et al. 2021).

2.2 | Global Climate Model Projections

This study utilised raw data from 10 GCMs provided by the Climate Change Dataset for Brazil—CLIMBra (Ballarin et al. 2023) (Table S1). These projections include daily data with a spatial resolution of 0.25°×0.25° for variables such as precipitation (pr), maximum temperature (tasmax), minimum temperature (tasmin), surface shortwave radiation (rss), near-surface wind speed (sfcWind) and relative humidity (hur). The projections are based on two climate scenarios: (a) SSP2–4.5, representing intermediate greenhouse gas emissions and (b) SSP5–8.5, representing high greenhouse gas emissions. The datasets cover the periods from 1980 to 2010, as well as future projections from 2015 to 2100.

For this study, historical observed data from the Brazilian Daily Weather Gridded Data (BR-DWGD) (Xavier et al. 2016) with a spatial resolution of 0.25°×0.25° and for the historical period of 1980–2010 was used to assess the quality of the climate model projections. This dataset has been applied and has demonstrated satisfactory performance in hydrological and climatological studies in Brazil, as reported by Ballarin et al. (2023), Da Silva et al. (2019) and Almagro et al. (2017).

2.3 | Bias Correction Using the Quantile Mapping (QM) Method

The QM method was employed for bias correction due to its effectiveness in adjusting climate model data, as demonstrated by Abbas et al. (2022), Anil and Raj (2022) and Heo et al. (2019). In this study, a QM code developed in RStudio was used, employing a downscaling technique through QM, utilising the qmap package, as proposed by Shrestha et al. (2017). The input data for the code included observed historical data from BR-DWGD for the period 1980–2010 and simulated historical data from each model for the SSP2–4.5 and SSP5–8.5 scenarios. The output consisted of bias-corrected future climate data adjusted according to these two scenarios.

These bias correction factors were applied to the future precipitation projections of the models for the period 2015 and 2100, assuming that the bias remains consistent under future conditions. Similarly, this correction method was applied to other variables, such as maximum and minimum temperature, relative humidity, wind speed and solar radiation, using the ratio between observed and simulated data during the reference period.

2.4 | Land Use and Land Cover Modelling (LCM)

The LCM tool in TerrSet software was used to quantify and map changes in each land use and land cover class (Clark Labs 2020). The LCM enables retrospective analysis of land cover and models potential transitions between classes, estimating land use and land cover changes over time intervals.

The study area is classified into six land use and land cover classes: Atlantic Forest, Caatinga, Pasture, Agriculture, Urban Infrastructure and Water Bodies. To model these changes, input data corresponding to the years 2000 (t_1), 2010 (t_2) and 2020 (t_3) were used. Land use and land cover transitions were defined based on transformations observed between t_1 and t_2, where changes were identified from one specific class to another. Seven land use and land cover transition classes were selected for modelling: Caatinga to Pasture, Caatinga to Agriculture, Caatinga to Urban Infrastructure, Atlantic Forest to Agriculture, Atlantic Forest to Pasture, Atlantic Forest to Urban Infrastructure and Agriculture to Pasture. The land use and land cover map was obtained from the MapBiomas Collection 7.0 with a 30 m resolution for the year 2010, using Google Earth Engine.

These transitions were chosen based on observed reductions in areas previously occupied by shrub vegetation as land for pasture, agriculture, urban zones and sugarcane cultivation expanded over the years analysed. When defining transition classes, we selected and tested explanatory variables that represent factors influencing land use and land cover changes. Previous studies commonly highlight key variables that significantly affect land use and land cover change trends, including distance to highways, proximity to water bodies, urban areas, slope and digital elevation models (Sadhwani et al. 2022; Preis et al. 2021; Silva et al. 2020; Xavier and Silva 2018). Building on these traditionally considered variables, this study also incorporated new predictors, such as climate variability and socioeconomic indices, which, though underexplored in regional studies, are crucial for understanding land use and land cover dynamics in watersheds. These additional variables are especially pertinent in northeastern Brazil, where climate and soil conditions heavily influence agricultural and urban expansion patterns. A comprehensive list of the explanatory variables tested is provided in Table S2.

The explanatory variables were selected based on Cramer's V test (Equation 1), embedded in the TerrSet module. This test assigns values ranging from 0 to 1, reflecting the degree of association between the explanatory variable and the defined transition classes. In this study, only variables with significant associations, reflected by Cramer's V values greater than 0.15, were considered for land cover modelling, following the recommendation by Hamdy et al. (2017).

$$V = \sqrt{\frac{1}{N}\frac{\chi^2}{\mathrm{Min}\{(M-1),(N-1)\}}} \tag{1}$$

where χ^2 is the χ^2 coefficient, M and N represent the number of rows and columns, respectively, and N is the total number of observations.

This study employed a Markov Chain to model land cover change probabilities, outlining transitions from t_2 to t_3. A validation was then conducted between the observed and simulated land use and land covers for t_3. Subsequently, a multilayer perceptron (MLP) neural network with 10000 iterations, as recommended by Rocha et al. (2024) and Mishra et al. (2014), was used to estimate future land use and land cover for three scenarios: 2030 (short-term), 2055 (mid-term) and 2085 (long-term). Validation of the model's projection against the observed land use and land cover was conducted using the Kappa Index of Agreement (KIA), which indicates the degree of agreement between the two maps, both in a general sense and on a category-by-category basis (Equation 2).

$$K = \frac{O-E}{1-E} \tag{2}$$

where O is the observed accuracy or the proportion of corresponding values (the diagonal of the matrix) and E is the expected proportion of matches on this diagonal, assuming an independent classification model derived from the observed row and column totals.

2.5 | SWAT Hydrological Model: Input Data, Simulation and Calibration

The soil and water assessment tool (SWAT) model (Arnold et al. 1998) was used to simulate streamflow responses to future climate change and land cover scenarios in the Capibaribe River basin for short-, medium- and long-term projections.

2.5.1 | Input Data

The hydrometeorological database consists of historical time series from 1985 to 2019, obtained from official agencies. Maximum and minimum temperature, solar radiation, relative humidity and wind speed data were retrieved from the National Institute of Meteorology (INMET) (http://www.inmet.gov.br/projetos/rede/pesquisa). Streamflow and rainfall data were obtained from the National Water Agency (http://www.snirh.gov.br/hidroweb). Descriptions of the meteorological, streamflow and rainfall stations are provided in Table S3.

The digital elevation model used was the ASTER Global Digital Elevation Model (GDEM), with a spatial resolution of 30 m, freely available on the Earth Data platform (https://earthdata.nasa.gov). The land use and land cover map corresponding to the t_2 period and the parameters for the vegetation characteristics of the Caatinga and Atlantic Forest biomes, following the recommendations of Fernandes et al. (2020).

Soil types were derived from the Agroecological Zoning of Pernambuco (Silva et al. 2001), available at https://geoinfo.dados.embrapa.br/catalogue/#/dataset/2993. Soil physical-hydrological characteristics, such as the number of horizons, root depth, percentages of silt, sand, clay, gravel, organic carbon, hydrological group, porosity, saturated hydraulic conductivity, available water capacity and erodibility factors, were obtained from the Brazilian Soil Information System (SISolos), available at https://www.sisolos.cnptia.embrapa.br (EMBRAPA 2018).

2.5.2 | Model Calibration and Validation

The historical rainfall and streamflow data used for model calibration and validation span from 1985 to 2019, covering a total of 35 years. The period from 1985 to 1991 was designated for model warm-up, 1992–2010 for calibration and 2011–2019 for

validation. Several classical metrics were used to evaluate model performance, including the Nash-Sutcliffe (NSE) efficiency, Pearson's coefficient of determination (R^2) and the percent bias (PBIAS) index. Table S4 provides the classification of modelling performance based on R^2, NSE and PBIAS values, as outlined by Moriasi et al. (2015).

In this study, monthly streamflow calibration was conducted automatically using the SUFI2 algorithm (Ashu and Lee 2023; Silva et al. 2022; Santos et al. 2021; Siqueira et al. 2021) within the publicly available SWAT Calibration and Uncertainty Procedures (SWAT-CUP) software (Abbaspour 2011). Parameters were adjusted for each station after several iterations, with 500 simulations per station. Subsequently, the most sensitive parameters in the modelling process were identified (Table 1), following the recommendations of Arnold et al. (2012) and Abbaspour (2015).

2.6 | Effects of Climate Change and Land Use/Cover on Hydrological Processes

The effects of climate change and land use and land cover on hydrological processes in the Capibaribe River basin were assessed using the validated SWAT model in combination with future land use and land cover scenarios. The model was executed for three distinct temporal scenarios: short-term (2015– 2044, using 2030 land use and land cover data), medium-term (2045–2074, using 2055 land use and land cover data) and long-term (2075–2100, using 2085 land use and land cover data). These simulation periods were selected to align with the timeline of the climate data analysis, ensuring consistency across the datasets. The year for each land use and land cover scenario was chosen as a midpoint within the respective simulation period. During these simulations, hydrological balance variables such as surface runoff, evapotranspiration and groundwater recharge were investigated and compared to the reference period. This analysis considered two emission scenarios: SSP2–4.5 and SSP5–8.5.

3 | Results

3.1 | Hydrological Modelling: SWAT Calibration and Validation

The selection of the most suitable parameters for each contributing area is presented in Table 2. At the beginning of the calibration process for each streamflow station, all 20 initial parameters were included. Subsequently, they were reduced based on those that exhibited the greatest influence during calibration, using sensitivity analysis conducted with SWAT-CUP. It is important to note that only the parameters using the replacement method (*v*) present the actual parameter values to be inserted into the models. For the

TABLE 1 | Parameters and ranges tested for model calibration.

Method/parameter	Description	Range	
r__CN2.mgt	Initial SCS runoff curve number for moisture condition II (dimensionless)	−0.2	0.2
v__ALPHA_BF.gw	Baseflow recession constant (days)	0	1
a__GW_DELAY.gw	Time delay for aquifer recharge (days)	−30	60
sv__GWQMN.gw	Threshold depth of water in the shallow aquifer required for return flow (mm)	0	1000
v__EPCO.bsn	Plant uptake compensation factor (dimensionless)	0	1
v__ESCO.bsn	Soil evaporation compensation factor (dimensionless)	0	1
v__CH_N2.rte	Manning's *n* value for the main channel ($s\,m^{-1/3}$)	0	0.3
v__CH_K2.rte	Effective hydraulic conductivity of the channel (mm/h)	0	5
r__SOL_AWC.sol	Available water capacity of the soil layer (dimensionless)	−0.25	0.25
r__SOL_K.sol	Saturated hydraulic conductivity (dimensionless)	−0.25	0.25
r__GW_REVAP.gw	Groundwater 'revap' coefficient (dimensionless)	−0.25	0.25
v__REVAPMN.gw	Threshold depth of water in shallow aquifer for 'revap' to occur (mm)	0.02	0.2
r__SLSUBBSN.hru	Average slope length (m)	−0.25	0.25
a__RCHRG_DP.gw	Deep aquifer percolation fraction (dimensionless)	−0.04	0.05
v__CANMX.hru	Maximum canopy storage (mm)	0	10
v__BIOMIX.mgt	Biological mixing efficiency (dimensionless)	0	1
r__SOL_Z.sol	Depth from soil surface to bottom of layer (dimensionless)	−0.25	0.25
r__SOL_ALB.sol	Soil albedo (dimensionless)	−0.25	0.25
v__RES_RR.res	Average daily release rate from the main reservoir (m^3/s)	0	1000
v__RES_K.res	Hydraulic conductivity of the reservoir bottom (mm/h)	0	1

Abbreviations: a = addition; r = multiplication; v = replacement.

TABLE 2 | Calibrated parameter values for the contributing areas of each streamflow station.

Method/parameter	Toritama	Limoeiro	Vitória de Santo Antão	Paudalho	São Lourenço da Mata
r__CN2.mgt	−0.338	−0.569	−0.065	−0.289	−0.261
v__ALPHA_BF.gw	0.233	0.040	0.996	0.00012	0.077
a__GW_DELAY.gw	−10.772	—	21.762	—	71.835
v__GWQMN.gw	160.15	2276.41	936.25	77.93	67.799
v__EPCO.bsn	0.131	—	—	—	1.142
v__ESCO.bsn	0.462	—	—	—	0.824
v__CH_N2.rte	0.362	—	—	0.072	0.304
v__CH_K2.rte	10.193	—	—	—	4.889
r__SOL_AWC.sol	0.236	—	0.138	0.7196	0.020
r__SOL_K.sol	−0.984	−0.995	−0.731	−0.956	−0.071
r__GW_REVAP.gw	0.237	0.221	0.339	—	0.115
v__REVAPMN.gw	1.322	—	—	—	6.805
r__SLSUBBSN.hru	0.157	—	0.497	0.543	0.057
a__RCHRG_DP.gw	—	—	—	—	−0.0102
v__CANMX.hru	—	—	3.463	—	4.302
r__SOL_Z.sol	−0.167	—	—	—	0.219
R__USLE_P.mgt	−0.417	—	—	—	−0.103
v__RES_RR.res	119.07 259.48	—	—	—	438.61
v__RES_K.res	−0.223 0.817	1.329	—	0.297	0.711

Abbreviations: a = Addition; r = multiplication; v = replacement.

other parameters, mathematical operations are required, based on the initial values, to determine the final parameter value.

Figure S1 shows the hydrographs of observed and calibrated streamflows, as well as the hyetograph of average monthly precipitation for each streamflow station. The model calibration for the basin was performed sequentially, that is, one station at a time, following the order: Toritama, Limoeiro, Paudalho, Vitória de Santo Antão and São Lourenço da Mata. At the end of each iteration for a given station, the model suggested new rankings and parameter ranges, which were updated for the next iteration in that contributing area. The results of the calibration and validation for all stations are presented in Table 3.

The results for the Toritama station show satisfactory correlation values between the simulated and calibrated streamflows, with $R^2 = 0.70$, NSE = 0.64 and PBIAS = −5.22 during calibration. However, the model performance decreases during the validation period (NSE = 0.41, $R^2 = 0.48$ and PBIAS = −34.64), indicating unsatisfactory performance. This suggests an overall satisfactory model fit during calibration but reduced accuracy during validation. Some extreme streamflow events at Toritama, such as the peaks observed in 2004–2005 and 2010–2011, were captured by the model, though not always with high precision, particularly, during the validation period. The model overestimated some peaks and underestimated others. It is noteworthy that during heavy rainfall periods, such as 2007/2008 and 2013/2014, observed streamflow data were either missing or incomplete, which may have influenced model performance.

At the Limoeiro station, the results were considered to be good for both calibration and validation, with significant improvements in performance indicators during validation. During the calibration period, there was a good correspondence between observed and calibrated streamflows, although the model tended to underestimate peak flows.

For Vitória de Santo Antão, the results demonstrate good performance in both calibration and validation, with high R^2 and NSE values. At the Paudalho station, calibration covered the period from 1992 to 2019, and the statistical results are satisfactory. During validation, the statistical parameters improved significantly, with R^2 reaching 0.89 and NSE at 0.84, reflecting a more accurate fit between observed and simulated streamflows. However, the PBIAS of −70.19 suggests a marked overestimation of flows during validation. Descriptive statistics also indicate a calibrated mean flow lower than the observed (5.67 vs. 4.98 m^3/s), with the model providing more conservative estimates of maximum and minimum values.

At the São Lourenço da Mata station, calibration and validation covered the period from 1992 to 2019. During calibration, the

coefficient of determination (R^2) was 0.79 and NSE was 0.76, indicating good model performance, while the PBIAS of −29.89 suggests a slight underestimation of flows. In the validation period, statistical parameters improved, with R^2 of 0.90 and NSE of 0.71, confirming the model's consistency in reproducing observed streamflows. The PBIAS of −1.04 during validation indicates that flow underestimation was significantly reduced.

Descriptive statistics show a calibrated mean flow higher than the observed (11.49 vs. 8.93 m^3/s) during calibration and a higher validated mean flow (13.89 m^3/s) during the validation period. Comparison of maximum and minimum values shows that the model reasonably captured flow peaks, despite a slight tendency to underestimate extremes. These results demonstrate that, despite some challenges, the model is effective in simulating streamflows in the São Lourenço da Mata basin, reflecting a satisfactory statistical fit.

3.2 | Future Land Use and Land Cover Scenarios

Figure 2 presents the major land use and land cover changes observed throughout the basin from 1985 to 2020. A significant transformation of agricultural and pasture areas is evident over the years. In the middle course of the basin, a notable land use and land cover transition from vegetation and agricultural crops to pasture, livestock and exposed soil—grouped as 'pasture' in this study—shows a 280% increase between the beginning and end of the analysed period. It is important to note that this basin plays a crucial role in Pernambuco's agricultural context, particularly, in the lower course, where sugarcane monoculture and the sugar-alcohol industry in the economically significant Mata Norte and Mata Sul regions have substantial regional importance, as highlighted by Pernambuco (2010). However, agriculture, which dominated the basin in 1985, experienced a noticeable shift in the Agreste region from the 1990s onwards, where the agricultural sector persisted but on a smaller scale due to the development of the Agreste clothing manufacturing hub.

Using Cramer's V values greater than 0.15 as a threshold, several variables were identified as significant, including the digital elevation model, slope, distance to water bodies and evaporation. On the other hand, variables related to distance from highways, socioeconomic factors and vegetation indices showed lower values and were considered less significant for predicting future land use and land cover in the region.

TABLE 3 | Statistical performance of the model for the contributing areas of the streamflow stations during calibration and validation.

	Toritama		Limoeiro		Vitória de Santo Antão		Paudalho		São Lourenço da Mata	
Statistics	**Calib.**	**Valid.**	**Calib.**	**Valid.**	**Calib.**	**Valid.**	**Calib.**	**Valid.**	**Calib.**	**Valid.**
R^2	0.70	0.48	0.62	0.90	0.78	0.80	0.66	0.89	0.79	0.90
NS	0.64	0.41	0.61	0.82	0.76	0.74	0.64	0.84	0.76	0.71
PBIAS	−5.22	−34.6	−5.78	−14.2	−23.1	10.90	−31.7	−70.1	−29.89	−1.04
Mean (m^3/s)	1.88	3.78	2.90	2.81	4.08	1.60	6.56	7.52	11.49	13.89
Maximum (m^3/s)	32.15	34.71	55.79	87.86	24.02	26.99	91.89	137.8	166.9	233.7
Minimum (m^3/s)	0.00	1.41	0.00	0.00	0.056	0.028	0.412	2.84	0.172	0.342
Standard deviation	3.26	5.03	6.42	9.05	3.02	3.07	5.75	13.60	18.07	25.59

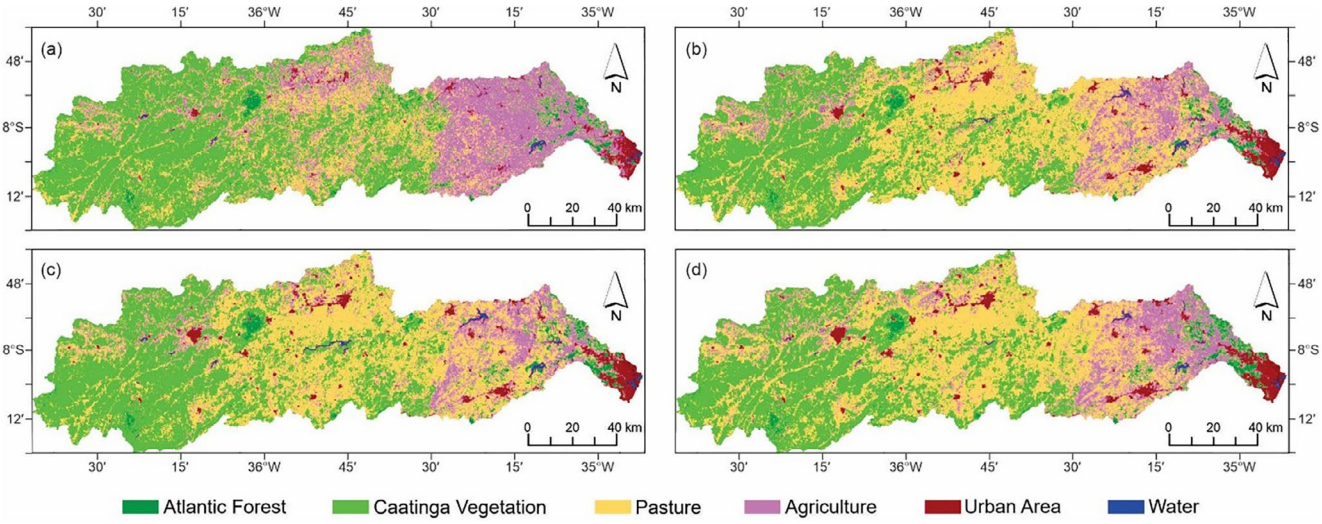

FIGURE 2 | Land use and land cover changes in the basin during the years: (a) 1985, (b) 2000, (c) 2010 and (d) 2020.

Table S5 presents the transition probability matrix for land use and land cover between t_2 and t_3, obtained using the Markov Chain model. The diagonal values represent the persistence percentages for each category, while the remaining values indicate the percentage of transition from one land cover category to another.

The transition matrix obtained from the Markov Chain model indicated that over 10 years, the Urban Infrastructure, Water Bodies, Atlantic Forest and Caatinga classes showed the highest probabilities of persistence, with values of 90.16%, 87.64%, 87.42% and 84.23%, respectively. In contrast, the Pasture class showed a persistence probability of 74.21%, while the Agriculture class had the lowest value, at 47.72%. Notably, the matrix revealed that approximately 27.01% of areas classified as Shrub Agriculture tend to be converted to pasture, a change pattern observed over the past two decades in the basin.

The KIA values for each class, representing the degree of agreement between the 2020 simulated map and the classified map, both in a general sense and by category, are shown in Table S6. Figure 3 illustrates the land use and land cover projections for 2030, 2055 and 2085. These projections suggest land use and land cover changes in the region, but not as drastic as those observed between 1985 and 2000, likely due to the region's development during that decade. The main projected change is the expansion of urban infrastructure, with some pasture and agricultural areas encroaching on Caatinga vegetation.

3.3 | Future Climate Change

To assess the climate projections for the study area, data from 10 GCMs were analysed, considering precipitation datasets for the short-term (2015–2044), medium-term (2045–2074) and long-term (2075–2100) periods under the emission scenarios SSP2–4.5 and SSP5–8.5. Figure 4 presents the correlation between the historical period for observed data compared to the raw data from climate models, both before and after bias correction. Table S7 provides the statistical performance of each climate model relative to the averages of the 10 models for the SSP2–4.5 (C_1) and SSP5–8.5 (C_2) scenarios.

The analysis of the statistical indicators suggests significant variation between the models compared to the average. The R^2 values are generally low, indicating a weak correlation between the simulated data and the ensemble mean. This implies that the models are producing statistically different results relative to the averages, which undermines confidence in simply using the mean precipitation values. The NSE values are mostly negative, suggesting that the models fail to efficiently reproduce historical data, providing evidence of large discrepancies between the model predictions and observed data. Additionally, the RMSE values are high, especially for models like ACCESS-ESM1-5 and CMCC-ESM2, indicating that the errors in the forecasts are considerable. This issue becomes more pronounced under the SSP5–8.5 scenario (C_2), where the error increases significantly.

The raw data from the models exhibit systematic errors, manifested by differences in seasonality and total precipitation, particularly, evident in the misrepresentation of the rainy season. This discrepancy is observed across all models, which tend to concentrate rainfall between February and May, contrary to the actual observed pattern in the Capibaribe River basin, where rainfall typically occurs between May and August. For instance, the IPSL-CM6A-LR model not only shows a difference in precipitation seasonality but also significantly overestimates the total precipitation, particularly, in MRR in May, exceeding 500 mm. Conversely, the ACCESS-ESM1 model consistently underestimates precipitation for all months across all regions. The differences in seasonality and total precipitation between the climate models and observed data have been similarly reported in previous studies using global circulation models, such as those by Tan et al. (2021), Takele et al. (2022), Santos et al. (2021) and Andrade et al. (2021). This highlights the clear need for bias correction methods to adjust the model outputs.

Figure 5 shows the projections of monthly precipitation for the short-, medium- and long-term periods. The results indicate

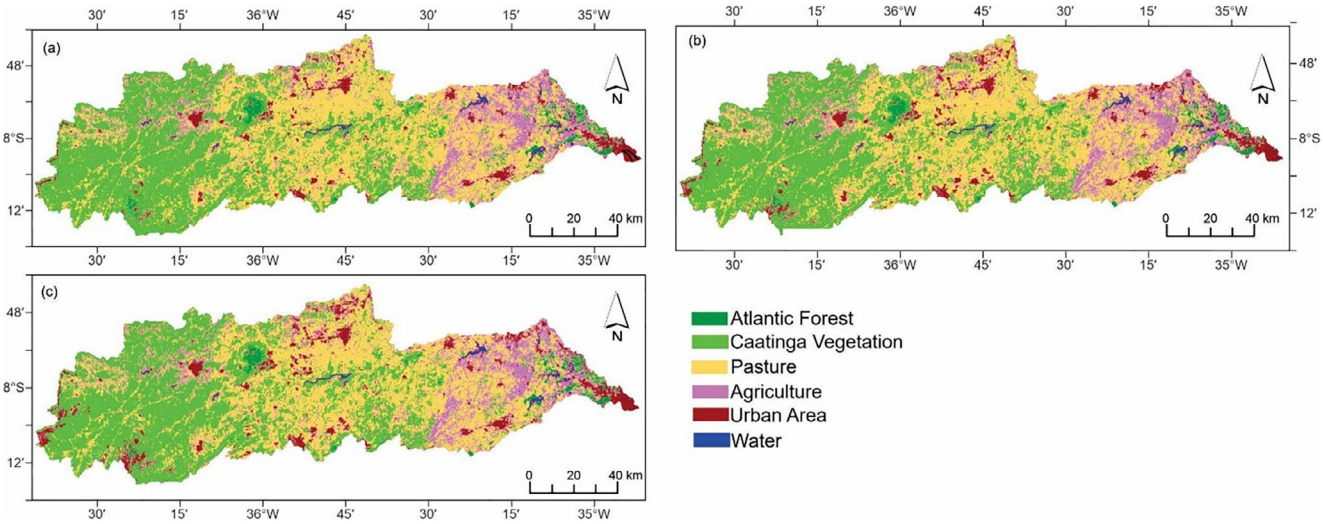

FIGURE 3 | Land use and land cover changes in the basin projected for 2030, 2055 and 2085.

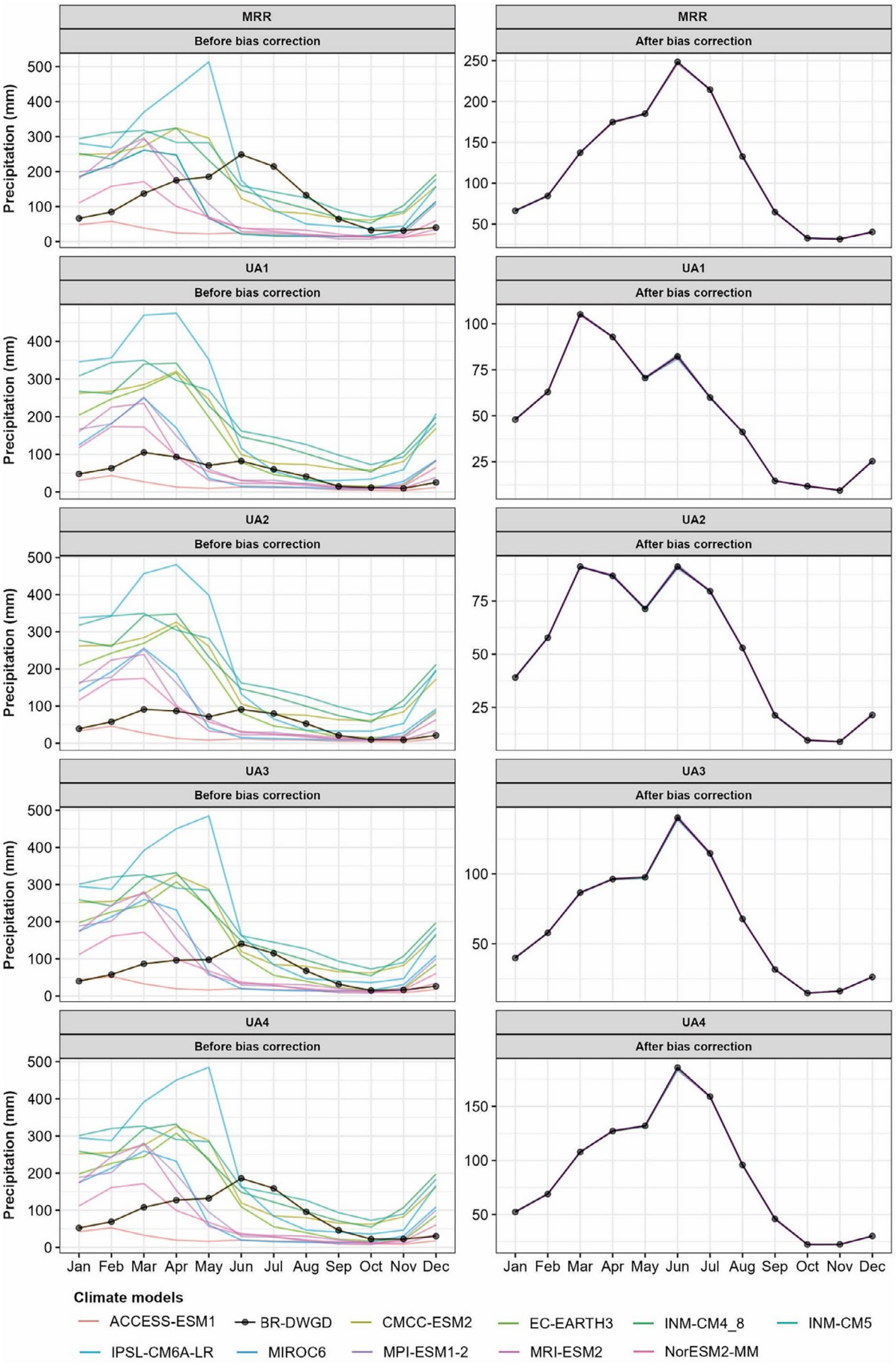

FIGURE 4 | Comparison of GCM climatological normals and observed data from 1980 to 2010, before and after bias correction.

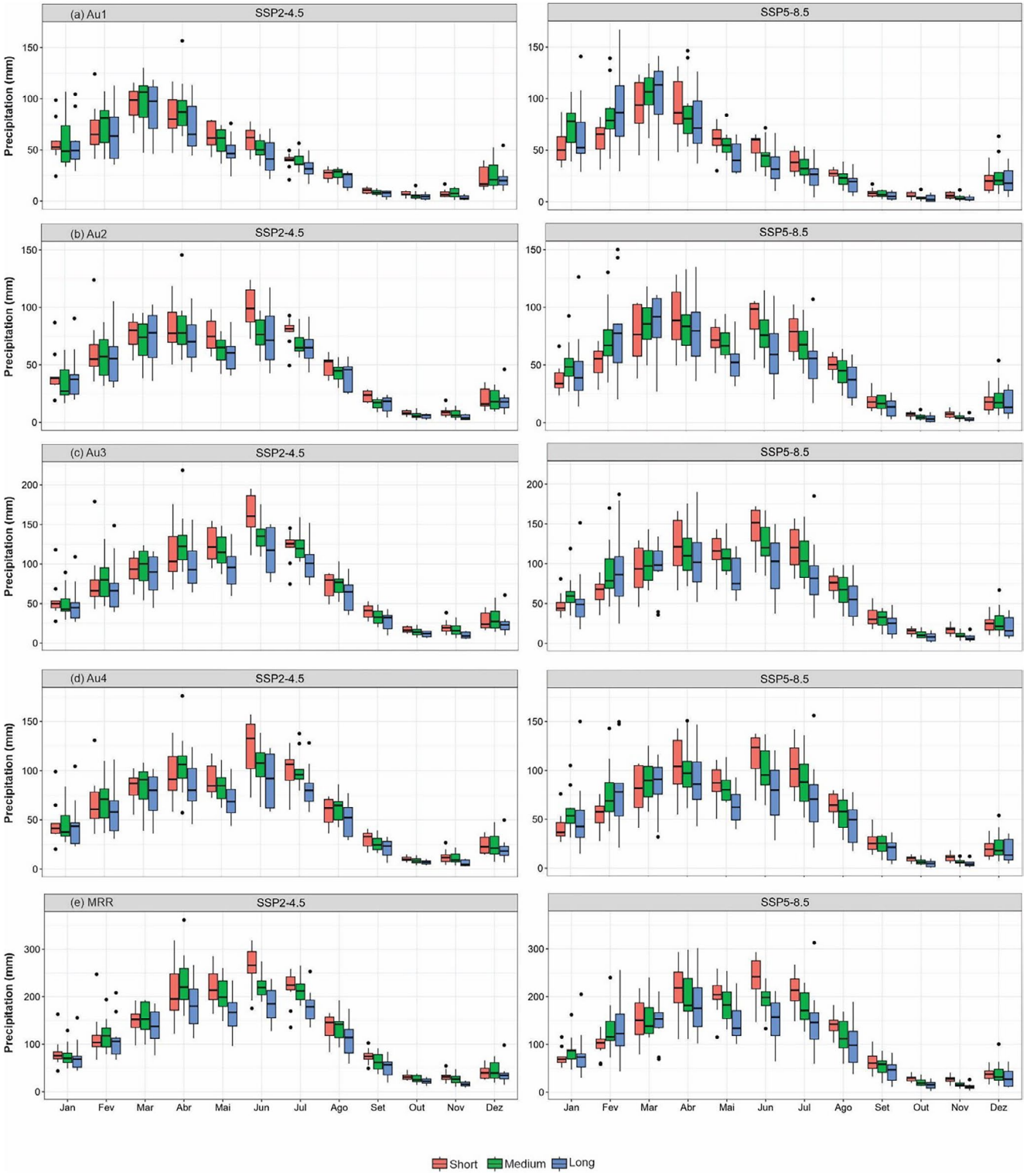

FIGURE 5 | Projections of monthly precipitation for short-, medium- and long-term periods.

that both scenarios show an increase in precipitation variability during the wettest months. In contrast, during the driest months, the difference in rainfall variability is less pronounced in both scenarios, suggesting greater stability and predictability in these conditions compared to the wetter months. These initial observations provide a framework for more detailed future analyses, offering valuable insights into potential future climate dynamics.

In MRR, which is the coastal area with the highest precipitation rates in the basin, the models showed significant variability in predictions for the wettest months. For example, in May, the precipitation ranged from 163 to 285 mm, while June varied from 175.23 to 319.21 mm. In contrast, the dry months showed smaller variations, such as in October (23.6–45.7 mm), November (16.81–54.28 mm) and December (25.5–65.5 mm). The analysis unit UA4, which has a slightly lower average rainfall than the

metropolitan region, showed variations in the wettest months from 67.8 to 175.6 mm in April and 109.7 to 195.26 mm in June. In the dry months, the variations ranged from 10.6 to 22.4 mm in October and from 9.7 to 38.33 mm in November.

In analysis unit UA1, which is located further inland, the wettest months showed variations of approximately 41.1–124 mm in February and 46.8–116.74 mm in April, while the dry months saw differences ranging from 5 to 10.5 mm in October. Similarly, in UA2, rainfall varied from 35.5 to 123.7 mm in February and from 50.13 to 118.7 mm in April, with dry month variations of 4.33 to 11.24 mm in October and 4.18 to 19.2 mm in November.

Figure 6 shows the projections of maximum and minimum temperatures for the climate models until the end of the century for each analysis unit. The temperature projections for both variables (minimum and maximum) indicate a considerable warming trend across all analysis units. The SSP2–4.5 scenario projects a gradual increase in minimum temperature over time for all areas, with the mean of the climate model projections suggesting a continuous rise until 2100. However, the increase is less pronounced compared to SSP5–8.5. This more pessimistic scenario projects a sharper rise in minimum temperature, especially from 2040 onward, where the difference between the two scenarios becomes more pronounced. By 2100, the minimum temperatures projected under SSP5–8.5 are significantly higher than those under SSP2–4.5.

Similarly, the projected maximum temperature follows a similar pattern, showing a progressive increase over time under the SSP2–4.5 scenario. The model means indicate a steady upward trend until the end of the century, with a more rapid and pronounced increase compared to SSP2–4.5. By 2100, the maximum temperatures under SSP5–8.5 are considerably higher.

3.4 | Effect of Climate Change and Land Use and Land Cover on Future Streamflows

Figures 7–9 present the mean streamflows from the 10 climate models and the range of variation under the SSP2–4.5 and SSP5–8.5 scenarios for each analysis unit (UA1, UA2, UA3, UA4 and MRR) in the short, medium and long term, across different climate scenarios and regions of interest. The results for each analysis unit in the short term are shown in Figure 7a–j. In the UA1 and UA4 regions under the SSP2–4.5 scenario, the projected maximum streamflows remain relatively low, not exceeding 40 m^3/s throughout the projected period. These moderate flows suggest that these regions may experience a less vulnerable hydrological regime under the intermediate emissions scenario, with fewer extreme changes. In contrast, the UA2 and UA3 regions exhibit much sharper flow peaks, reaching between 200 and 300 m^3/s. These high values indicate that these areas could be at greater risk of flooding during extreme precipitation events, even under the more moderate emissions scenario. The results for the MRR show even higher flows, with peaks exceeding 700 m^3/s, highlighting this region's particular vulnerability to large water volumes during seasonal events. The range of variation, indicated by the shaded area, also suggests that the uncertainty surrounding the projections is higher for this region.

In the analysis of the SSP5–8.5 scenarios, which represent a more extreme scenario of high emissions, all analysis units show an intensification of streamflow events. This suggests that with rising global temperatures and increased greenhouse gas emissions, the hydrological behaviour becomes more variable and extreme. The UA1 and UA4 regions under SSP5–8.5 exhibit higher peak flows compared to SSP2–4.5, although the maximum values remain below 50 m^3/s. This indicates that while these regions may not experience drastic changes in flow under the extreme scenario, there will still be an increase in the intensity of hydrological events. The UA2 and UA3 regions continue to show significant variability in flow, with peaks exceeding 250 m^3/s. The difference between the two scenarios is evident, with more frequent and intense peaks occurring under SSP5–8.5. The range of uncertainty also increases, suggesting that these regions could face more severe hydrological events as global emissions rise. For the MRR under the SSP5–8.5 scenario, the results show an extreme intensification of peak flows, with values surpassing 800 m^3/s. This region appears to be the most vulnerable to climate change, with a substantial increase in both the average flows and the associated uncertainty. The heightened variability indicates a much higher risk of extreme events, such as floods and flash floods.

The results for each analysis unit in the medium term are shown in Figure 8a–j. In the SSP2–4.5 scenario, there is a relatively consistent pattern over time, with peaks occurring regularly. In UA1 and UA4, the peaks remain moderate, not exceeding 60 m^3/s, suggesting a stable response to climate change. In the UA2 and UA3 regions, the peaks are significantly higher, reaching 500 and 700 m^3/s, respectively. These peaks indicate an increase in extreme events, with high variability, especially in the MRR, where flows surpass 1000 m^3/s. Under the SSP5–8.5 scenario, the intensity and frequency of peaks increase considerably in all regions. In UA1 and UA4, flows reach higher values, nearing 60 m^3/s, while in UA2 and UA3, the peaks reach up to 600 m^3/s. The MRR continues to be the most vulnerable, with peaks exceeding 800 m^3/s. This scenario suggests a future with more frequent extreme hydrological events, particularly, in the more sensitive regions such as UA2, UA3 and MRR.

The long-term results for each analysis unit are shown in Figure 9a–j. In the SSP2–4.5 scenario, UA1 shows peaks up to 50 m^3/s throughout the period, indicating a relatively stable and moderate flow trend. Meanwhile, UA2 presents peaks reaching 350 m^3/s, highlighting greater variability and susceptibility to extreme hydrological events, although to a more moderate degree compared to the SSP5–8.5 scenario.

The results for UA3 show high variability in streamflows, with peaks reaching 500 m^3/s, suggesting that this region may face intense flood episodes and more significant fluctuations in flow projections. UA4 exhibited more stable flows, with peaks below 50 m^3/s, similar to UA1, indicating that these regions may experience less drastic changes in their hydrological regimes. In this scenario, the MRR stood out for having the highest peaks among all regions, with values reaching 1000 m^3/s. This highlights the particular vulnerability of the MRR to extreme flow events, even under an intermediate emissions scenario.

In the SSP5–8.5 scenario, peak flows in UA1 and UA4 were slightly higher than those in the SSP2–4.5 scenario, reaching

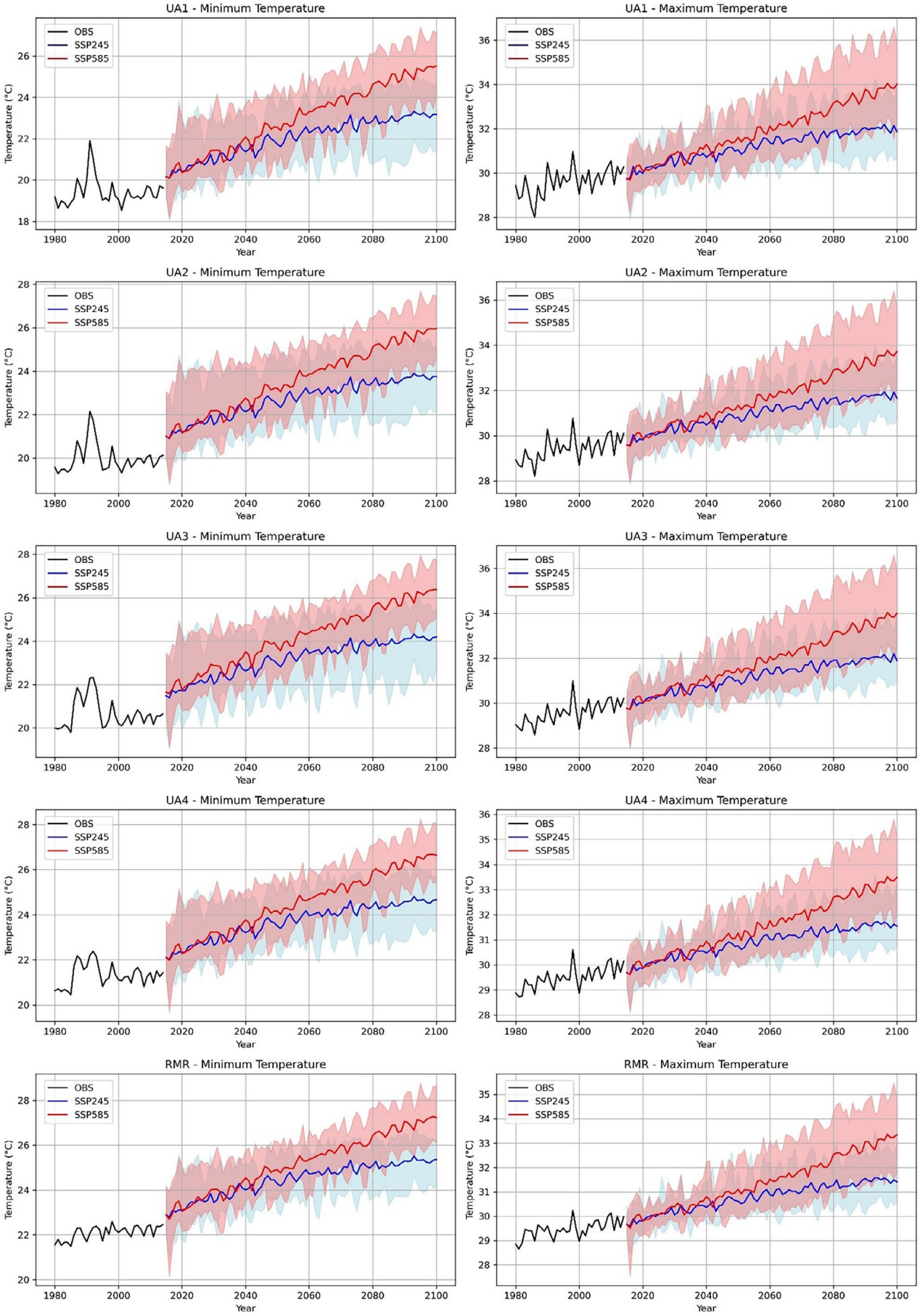

FIGURE 6 | Projections of monthly precipitation for short, medium and long-term periods.

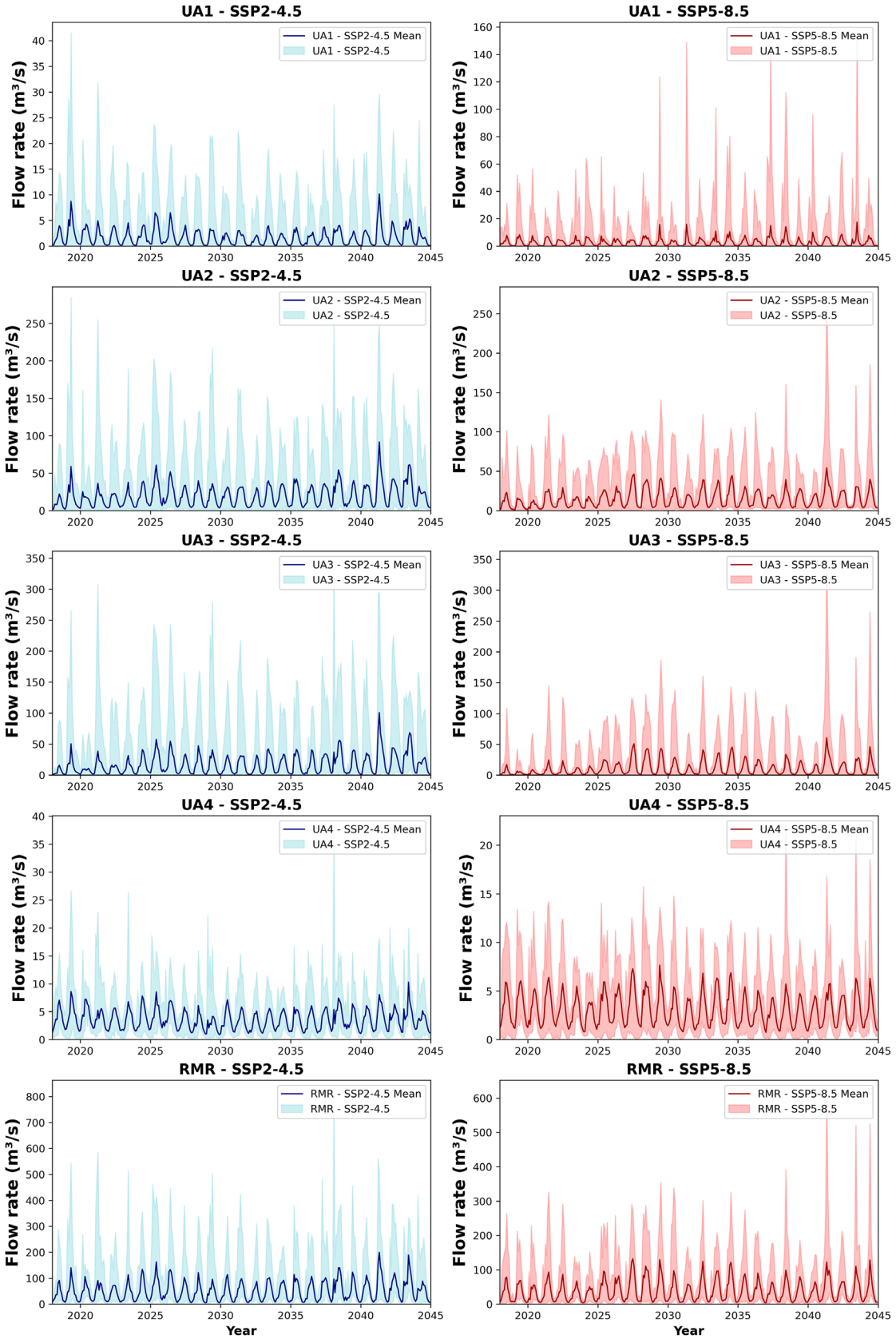

FIGURE 7 | Estimated average streamflows and the range of variation from the 10 climate models for the analysis units in the short term.

values close to 50 m^3/s. While the difference is not extreme, these values indicate an intensification of hydrological events. UA2 and UA3 showed the highest values in the basin, with peaks of up to 500 m^3/s in UA2 and 700 m^3/s in UA3. The amplitude and variability of hydrological events increased considerably, reflecting greater uncertainty and vulnerability in these regions under the higher emissions scenario. The MRR continued to experience the highest peaks, exceeding 1000 m^3/s. The frequency and

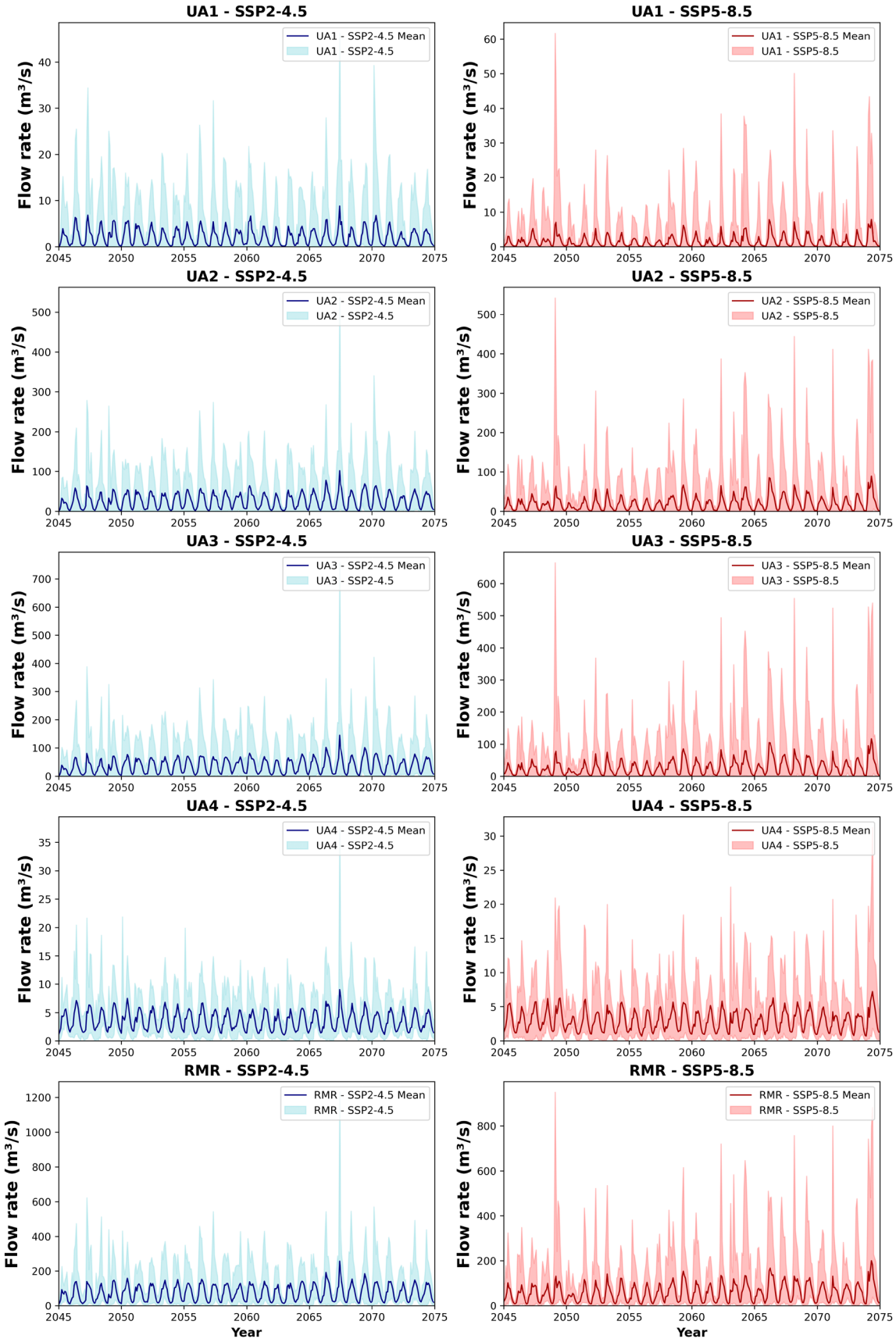

FIGURE 8 | Estimated average streamflows and the range of variation from the 10 climate models for the analysis units in the medium term.

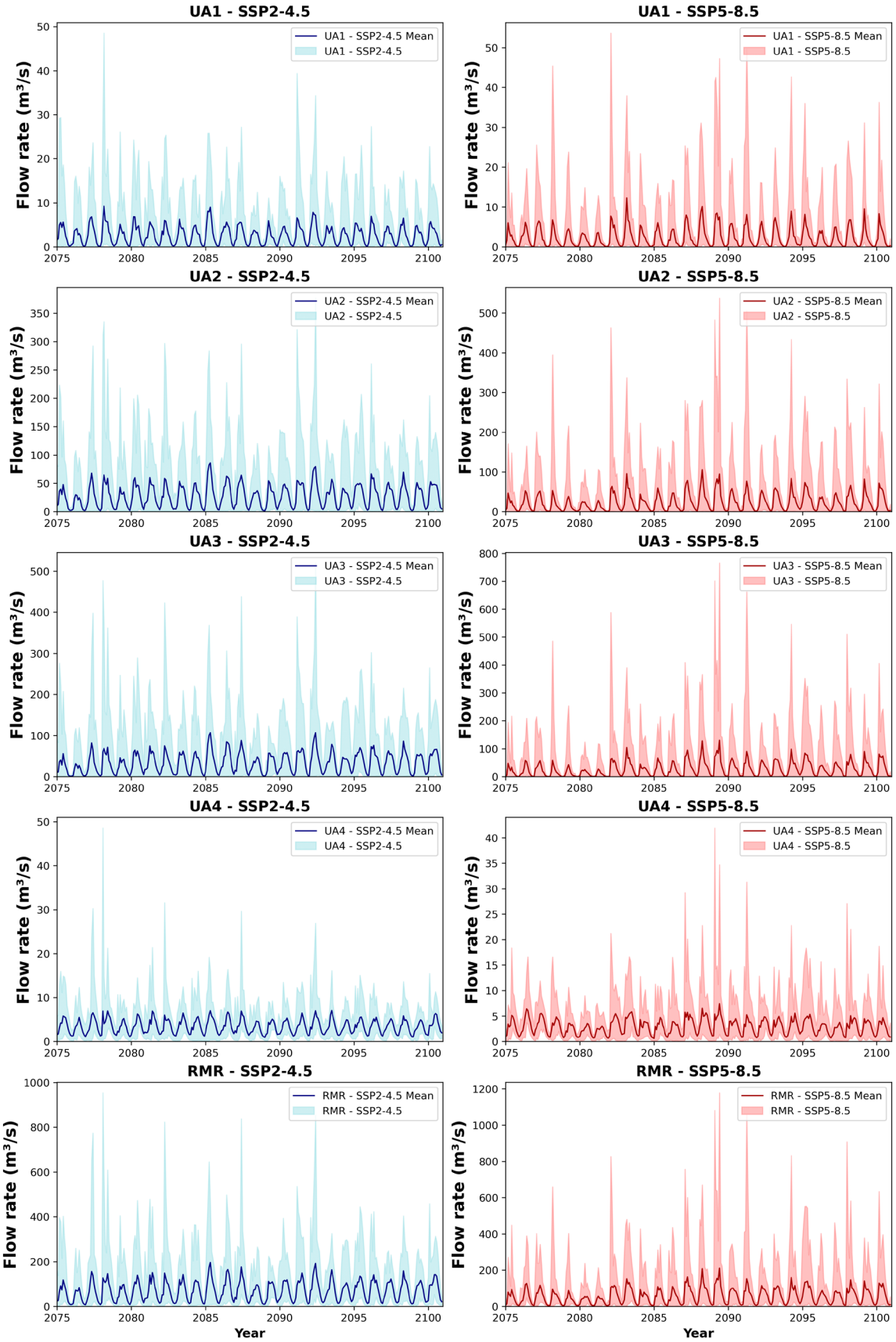

FIGURE 9 | Estimated average streamflows and the range of variation from the 10 climate models for the analysis units in the long term.

intensity of these events indicate that this area will be highly exposed to flood risks and other extreme hydrological events by the end of the century.

3.5 | Vegetation Cover Responses to Streamflow Under Different Future Climate Scenarios

To assess how streamflow behaves in the watershed based on each land use and land cover type, Figure 10a–c present surface runoff projections for the short, medium and long term across five land use and land cover classes under the SSP2–4.5 (blue) and SSP5–8.5 (orange) climate scenarios, in comparison to observed data (red points) and future projections based on the average of the 10 climate models (blue points). In urban areas, surface runoff is consistently the highest compared to other land use and land cover classes. This is expected due to the high level of soil impermeability, which prevents water infiltration. In the medium term, the difference between the SSP2–4.5 and SSP5–8.5 climate scenarios becomes more pronounced, with SSP2–4.5 showing higher runoff and greater variability. This highlights the high sensitivity of urban areas to climate change in the medium term. In the long term, urban areas continue to exhibit the highest runoff values, with the difference between the SSP2–4.5 and SSP5–8.5 scenarios becoming even more evident. This trend underscores the increasing sensitivity of these areas to climate change over time, particularly, under the more severe SSP5–8.5 scenario.

In the Caatinga class, runoff is very low in both scenarios, with little variation between them and even smaller values in the more distant time horizons. This is expected due to the sparse vegetation cover and higher infiltration and evaporation rates in the Caatinga biome. The Atlantic Forest also shows low runoff values, with slightly more variation compared to the Caatinga, but with no significant differences between the SSP2–4.5 and SSP5–8.5 scenarios. In the long term, the Caatinga and Atlantic Forest classes maintain relatively stable and low runoff levels across the scenarios and time periods. The impact of climate change in these areas appears to be much less pronounced compared to urban and agricultural areas. These vegetative classes seem less affected by climate change in the medium term, maintaining almost stable surface runoff.

Agricultural and pasture areas exhibit intermediate runoff values. Although agricultural areas can facilitate infiltration, some intensive agricultural practices contribute to increased runoff, a behaviour similarly observed in pasture areas. Soil compaction and rainfall conditions influence both land-use classes in similar ways. In the long term, the SSP5–8.5 scenario shows greater variation in runoff for these classes, suggesting that the impacts of climate change become more evident in this scenario and time horizon.

In summary, urban areas stand out with the highest runoff and the greatest range of variation, especially under the SSP5–8.5 scenario in the short term and the SSP2–4.5 scenario in the long term. This indicates that urban areas are more sensitive to climate change. In contrast, the Caatinga and Atlantic Forest classes show low runoff, with minimal differences between the scenarios, while agricultural and pasture areas show intermediate runoff levels.

Table 4 shows the relative change (%) in surface runoff for different land use and land cover classes across three distinct time horizons. Urban areas exhibit the most significant changes, with substantially higher runoff from the short term, particularly, under the SSP2–4.5 scenario. In the medium and long term, the surface runoff depth tends to decrease across all classes, except for the Atlantic Forest, which remains stable. Pasture and agricultural areas follow a similar pattern, with moderate increases in the short term under the intermediate scenarios but show more pronounced decreases in the medium and long term, especially under the SSP5–8.5 scenario. The Caatinga areas also show a significant change compared to what has been observed in recent years. The average water depth, which was 7.36 mm, tends to decrease significantly in the short term under the intermediate scenario, reaching a 94.4% reduction in the high-emission scenario in the long term. Overall, the most pronounced changes occur in urban, agricultural, pasture and Caatinga areas, while the Atlantic Forest remains more resilient.

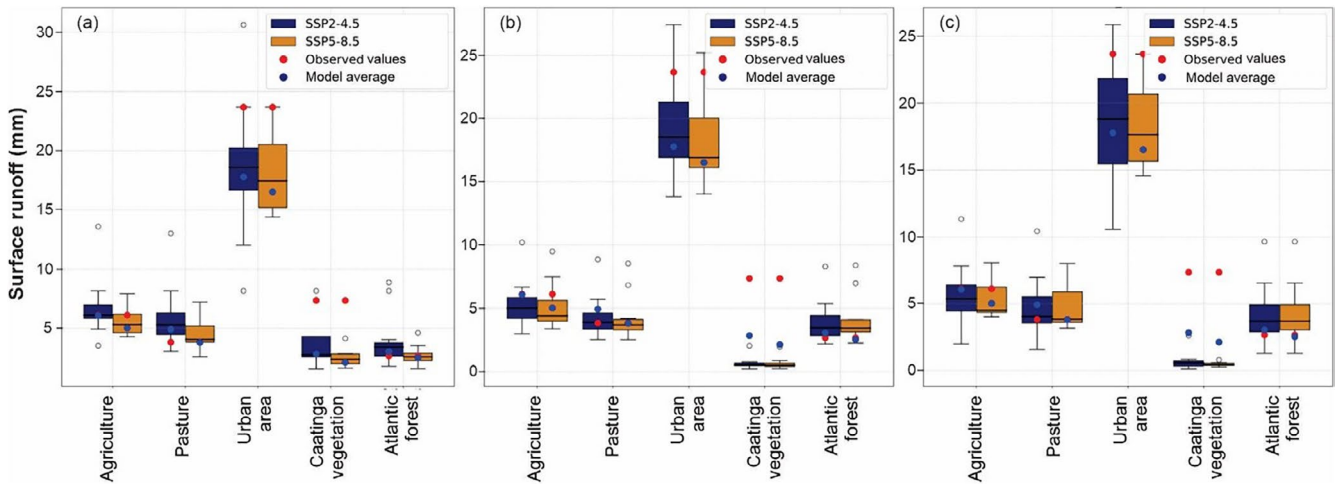

FIGURE 10 | Surface runoff for land use and land cover classes for (a) short term, (b) medium term and (c) long term under SSP2–4.5 and SSP5–8.5 scenarios.

TABLE 4 | Relative change (RC, %) in surface runoff (Q, mm) for land use and land cover classes in the short-, medium- and long-term periods under climate change scenarios.

		Short-term				Medium-term				Long-term			
		SSP2–4.5		SSP5–8.5		SSP2–4.5		SSP5–8.5		SSP2–4.5		SSP5–8.5	
LULC	Q_{obs} (mm)	Q (mm)	RC (%)	Q (mm)	RC (%)	Q (mm)	RC (%)	Q (mm)	RC (%)	Q (mm)	RC (%)	Q (mm)	RC (%)
Agriculture	6.08	6.12	0.66	5.03	−17.3	4.30	−29.3	3.90	−35.9	4.68	−23.0	4.52	−25.6
Pasture	3.83	4.93	28.72	3.81	−0.52	3.43	−10.4	3.31	−13.6	3.73	−2.6	3.85	0.52
Urban area	23.67	17.78	−24.9	16.52	−30.2	17.8	−24.8	16.9	−28.8	16.9	−28.4	17.17	−27.4
Caatinga	7.36	2.84	−61.4	2.13	−71.1	0.50	−93.2	0.53	−92.8	0.59	−91.9	0.41	−94.4
Atlantic Forest	2.67	3.04	13.86	2.53	−5.2	3.20	19.8	3.28	22.9	3.41	27.7	3.41	27.7

Table 5 provides a statistical assessment of the projected surface runoff from the models for the three time periods, compared to the observed streamflow period of the basin. Over time, a decrease in the mean runoff in mm is observed for both scenarios analysed, SSP2–4.5 and SSP5–8.5. In the short term, the averages are 6.94 and 5.96 mm, respectively, dropping to 4.89 and 4.95 mm in the long term. This suggests a trend of declining projected runoff over the years. The standard deviation (SD), which reflects the dispersion of the data relative to the mean, remains relatively stable across scenarios and periods, with values ranging from 6.02 to 6.44 mm. This indicates that the variability in projected runoff is similar across the different time horizons.

The mean absolute deviation (MAD), which measures the dispersion of values relative to the mean, follows a trend similar to the SD, with values between 4.07 and 4.78 mm, as expected. The coefficient of variation (CV), representing the ratio of the SD to the mean, shows relatively low variability, with a slight upward trend in the long term, particularly, under the SSP5–8.5 scenario, where the CV reaches 1.29. This indicates that while the variability of the data remains small relative to the mean, it may increase in more extreme future scenarios. The mean squared error (MSE), which quantifies discrepancies between model projections and historical data, increases from the short term to the long term, with values of 11.28 in the short term for SSP2–4.5, rising to 18.83 in the long term for SSP5–8.5.

Table 6 presents the water balance variables for different land use and land cover classes under the SSP2–4.5 and SSP5–8.5 scenarios. As expected, surface runoff in urban areas is the highest among all land use and land cover classes. This is due to soil impermeability, which prevents water infiltration. The decrease in runoff over time reflects the corresponding reduction in precipitation over these areas in both scenarios and time horizons. Agricultural and pasture areas exhibit intermediate runoff, lower than urban areas but still significant. The increase in runoff over time is noticeable, particularly, in the long term. The intensification of runoff in these areas indicates a reduction in water infiltration capacity, which may result from increased soil compaction or inadequate land management practices in response to climate change.

The Caatinga and Atlantic Forest areas display the lowest surface runoff values, due to the higher infiltration capacity of natural vegetation, evapotranspiration and ground cover. Regarding groundwater, the Atlantic Forest shows the highest infiltration rates for groundwater recharge, as expected due to its dense ecosystem and vegetation with a high water absorption capacity. Agricultural areas also exhibit good rates of groundwater recharge, although at lower levels compared to the Atlantic Forest. Pasture and Caatinga areas have lower groundwater recharge values (GWQ), indicating that much of the water is not infiltrating deeply into the soil. This may be due to soil compaction, reduced vegetation cover and lower precipitation in these regions of the basin.

Evapotranspiration in the Atlantic Forest area is consistently high across the time horizons, reflecting the abundant vegetation in this biome. The amount of water that evaporates

TABLE 5 | Statistical evaluation of projected runoff by the models in the short, medium and long term for the SSP2–4.5 and SSP5–8.5 scenarios compared to the observed historical period of the basin.

Time period	Scenario	Mean	SD	MAD	CV	MSE	RVR
Short term	SSP2–4.5	6.94	6.21	4.34	0.89	11.28	−0.09
	SSP5–8.5	5.96	6.02	4.23	1.01	15.95	−0.27
Medium term	SSP2–4.5	5.84	6.83	4.78	1.17	17.03	−0.28
	SSP5–8.5	5.58	6.44	4.51	1.16	19.67	−0.30
Long term	SSP2–4.5	4.89	6.19	4.02	1.26	18.71	−0.24
	SSP5–8.5	4.95	6.28	4.07	1.27	18.83	−0.21

TABLE 6 | Water balance variables from the SWAT model for each land use and land cover class in the short-, medium- and long-term under the SSP2–4.5 and SSP5–8.5 scenarios.

		SSP2–4.5				SSP5–8.5			
LULC	Periods	PREC (mm)	SURFQ (mm)	GWQ (mm)	ET (mm)	PREC (mm)	SURFQ (mm)	GWQ (mm)	ET (mm)
Agriculture	S	1003.8	93.2	433.9	339.8	876.6	69.7	364.3	332.2
	M	957.2	49.9	395.7	352.0	938.5	52.5	349.3	379.2
	L	960.9	63.4	386.6	359.3	975.0	68.8	377.7	382.6
Urban area	S	1271.5	510.7	306.1	412.1	1120.3	420.9	270.9	390.9
	M	1037.3	363.0	200.7	382.5	1015.3	357.1	178.7	399.0
	L	950.9	314.6	155.7	359.5	967.0	333.3	144.2	369.1
Atlantic Forest	S	1330.5	39.32	832.9	407.7	1172.8	29.2	710.1	388.6
	M	1248.2	8.1	735.5	430.3	1222.9	8.7	668.4	464.0
	L	1248.7	8.2	737.2	426.93	1257.2	8.7	736.2	437.3
Pasture	S	760.1	82.3	166.4	354.8	657.4	43.2	122.0	330.9
	M	761.6	39.8	186.9	347.1	750.2	45.1	150.7	366.4
	L	769.7	49.6	189.2	345.4	792.3	60.7	186.4	345.3
Caatinga vegetation	S	644.5	53.9	123.6	325.6	581.5	19.0	81.5	300.3
	M	661.3	30.7	109.1	320.8	652.0	39.4	78.1	338.8
	L	633.7	34.8	130.8	313.4	668.5	46.9	132.8	328.2

Abbreviations: L = long-term; M = medium-term; S = short-term.

and transpires from plants is significant in these regions. Agricultural and pasture areas show intermediate evapotranspiration values, which can be influenced by soil management practices and crop conditions.

Urban areas exhibit the highest sediment production. Erosion and sediment transport are exacerbated by the lack of vegetation cover and urbanisation, which promotes soil movement during precipitation events. Sediment production in agricultural areas is also high, where intensive farming and the absence of soil conservation practices can contribute to a significant increase in erosion. While pasture areas have lower sediment production compared to agriculture, it remains significant. Soil compaction and inadequate vegetation cover can lead to erosion and sediment transport. The Atlantic Forest shows the lowest sediment production, highlighting the biome's ability to protect soil from erosion. Dense vegetation and permeable soil play a crucial role in sediment retention. Comparing the different land use and land cover classes, urban areas have the highest surface runoff, as well as high evapotranspiration and sediment production. The Atlantic Forest, in contrast, stands out for its low sediment production, higher groundwater infiltration and high evapotranspiration.

In this more severe scenario, it can be observed that the land use classes tend to experience reduced precipitation, leading to decreases in surface runoff, evapotranspiration, groundwater recharge and slight variations in sediment production. When comparing water balance variables between the two scenarios, average precipitation across all land use and land cover classes is slightly lower in SSP5–8.5 compared to SSP2–4.5, except in the long term, where the values converge. Surface runoff is

consistently higher in SSP2–4.5, suggesting that the SSP5–8.5 scenario tends to reduce the amount of water flowing directly on the surface. Groundwater recharge is generally higher in SSP2–4.5, except for the pasture class, where SSP5–8.5 shows elevated values. Evapotranspiration is slightly higher in SSP5–8.5, which may be explained by increased temperatures and higher water demand in the more severe scenario. Sediment production decreases in both scenarios over time and is generally lower in SSP5–8.5. These differences indicate that the SSP5–8.5 scenario, associated with more severe climate conditions, leads to reduced precipitation and surface runoff, along with higher evapotranspiration. Sediment production also declines, possibly due to fewer intense precipitation events.

4 | Discussion

This study analysed future streamflow behaviour and different land use and land covers in a basin located in the Atlantic Forest/Caatinga ecotone in northeastern Brazil. The coupling of climate models, land use and land cover estimation and hydrological modelling for the Capibaribe River basin yielded satisfactory results, as also reported by Xue et al. (2022), Wang et al. (2022), Anil and Raj (2022), Abbas et al. (2022), Song et al. (2021) and Shrestha et al. (2017). This methodology successfully captured the responses of streamflow behaviour and water balance for the various land use and land covers of the two studied biomes, enabling the development of adaptive strategies for preserving vegetation cover in the face of climate change.

4.1 | Assessing Land Use and Land Cover Change

The Capibaribe River basin has undergone natural and anthropogenic transformations in recent years. To study and simulate future transformations, an initial analysis was conducted on the changes that occurred over the past decades (1985–2020). A notable aspect of this basin was the growth of urban areas between 1985 and 2000. During this period, there was a significant expansion of urban areas, particularly, in the lower course near the river's mouth, driven by the growth of cities such as Recife, Abreu e Lima, Camaragibe and São Lourenço da Mata, which form the MRR. Additionally, cities in the upper course of the Capibaribe, such as Santa Cruz do Capibaribe and Toritama and in the middle course, such as Caruaru, Limoeiro and Vitória de Santo Antão, which form part of the textile hub or commercial expansion of agricultural products, also experienced notable growth.

The data suggest a continuous increase in urban centres, driven by the region's population growth and industrialisation. This results in demand for housing that tends to occupy the peripheral areas of each urban centre, as reported by Xavier and Silva (2018). The results also highlight a reduction in the vegetation fragments of the Caatinga and Atlantic Forest biomes, which have seen portions of their areas converted into pasture. However, some remnants within the basin still preserve elements of these ecosystems' original fauna and flora.

In summary, a significant portion of the vegetation cover has been replaced by activities such as polyculture, pasture, livestock farming and exposed soil areas. Vegetation-covered areas have declined over time, with a 51% reduction in tree cover and a 17% decrease in shrub cover. This scenario is primarily driven by the intensification of sugarcane monoculture, along with the expansion of areas for maize, beans and pineapple cultivation (classified under agriculture) and pasture expansion.

4.2 | Assessing Streamflow Responses to Future Climate Change and Land Use and Land Cover

The bias correction method applied to the raw data proved effective, as it satisfactorily adjusted precipitation and successfully represented the seasonality of rainfall in the basin. The modelling results for the Toritama station suggest that the model had more difficulty predicting streamflows with the same precision outside the calibration interval. Statistically, this result is consistent with the findings from Ferreira (2020) and Diaz (2021). Ferreira (2020) conducted two calibrations for different periods at the station, achieving good values for calibration but unsatisfactory values during validation. Diaz (2021) reported $R^2 = 0.20$ and NSE = 0.14, which are considered unsatisfactory based on the adopted classification. In Ferreira's (2020) best calibration for Limoeiro, an R^2 of 0.691 and an NSE of 0.672 were found, with validation results showing an R^2 of 0.83 and an NSE of 0.646. These results align with the present study's findings, which achieved even better statistical values during the validation period. Diaz (2021) reported lower calibration values, with an R^2 of 0.34 and NSE of 0.19.

The model recorded some high-flow events, which corresponded well with rainfall during the period, yet the observed data did not exhibit the same flow peaks. This discrepancy could affect the calibration process due to potential measurement equipment failures, logistical difficulties in accessing the station during extreme weather events or even loss of historical data (Frade et al. 2024). Additionally, the presence of the Poço Fundo and Engenheiro Gercino Pontes reservoirs influenced the flow regime, as they are used to store water during periods of high precipitation and release it during dry periods, thereby regulating flow in a controlled manner (Andrade et al. 2021). The combination of missing observed data and the unquantified influence of the reservoirs increased the uncertainties in flow predictions.

Santos et al. (2021) reported statistical values of $R^2 = 0.72$, NSE = 0.71 and PBIAS = −23.73 for calibration, while Diaz (2021) obtained $R^2 = 0.81$ for calibration, $R^2 = 0.54$ for validation, NSE = 0.8 for calibration and NSE = −0.08 for validation. For the Paudalho station, Ferreira (2020) found $R^2 = 0.67$ and NSE = 0.43 for the first calibration and $R^2 = 0.626$ and NSE = 0.621 for the second calibration. $R^2 = 0.53$ and NSE = 0.064 were reported for the first validation, while the second validation yielded much better results, with $R^2 = 0.94$ and NSE = 0.862. Diaz (2021) reported unsatisfactory calibration statistics, with $R^2 = 0.20$ and NSE = 0.10. For São Lourenço da Mata, Ferreira (2020) reported $R^2 = 0.66$ and NSE = 0.56 in the best calibration and $R^2 = 0.641$ and NSE = 0.63 in the best validation. Diaz (2021) found calibration values of $R^2 = 0.61$ and NSE = 0.57.

The comparison between SSP2–4.5 and SSP5–8.5 scenarios reveals that all analysis units are likely to experience significant

changes in flow rates under the higher emissions scenario. Regions such as UA2, UA3 and, particularly, the MRR, display greater vulnerability to extreme events and uncertainties in hydrological projections. On the other hand, regions like UA1 and UA4 show more moderate variation, though they will still face an increase in flow intensity under the SSP5–8.5 scenario. These results underscore the need for effective climate change mitigation policies and adaptation strategies in vulnerable regions.

A trend of consistent seasonal peaks was observed, suggesting that flow rates follow a relatively stable pattern with well-defined annual fluctuations. In the long term, these projections highlight the growing impact of climate change, with marked differences between emission scenarios. The regional variation and the magnitude of flow peaks emphasise the importance of localised adaptation policies to mitigate future impacts.

This study encountered significant challenges due to the inherent complexity of the Capibaribe River basin. The basin exhibits a unique combination of climatic variability, ranging from semiarid to coastal regions, along with diverse land use and land cover patterns, including pastures, agriculture and rapidly expanding urban areas. Moreover, agricultural practices and accelerated urbanisation have further strained the region's water resources. Climate change projections often struggle to accurately capture precipitation and streamflow patterns in such a highly heterogeneous basin, adding another layer of complexity. Nevertheless, these challenges make the research distinctive, providing valuable insights for other regions with similarly diverse characteristics. This study underscores the importance of adopting region-specific approaches when addressing the impacts of climate change on water resources.

4.3 | Model Uncertainties and Limitations

A primary source of uncertainty in this study stems from the GCMs. The raw outputs from these models often exhibit significant biases in both pattern and amount when compared to local observations, a well-documented challenge in climate impact studies. Therefore, the application of a bias correction method is not only a common practice but an essential step to remedy these systematic errors before the data can be used for hydrological modelling (Ballarin et al. 2023; Xue et al. 2022; Wen et al. 2021). As the performance metrics in Table S7 indicate, the models exhibit low correlation and negative NSE values when assessed at a daily time step. This outcome is largely expected due to the inherent stochastic nature of GCMs, which are designed to reproduce the statistical properties and long-term climatology of a region rather than to precisely replicate observed weather events on a specific day. The low daily performance, therefore, reflects a temporal mismatch in precipitation events, a known characteristic of GCM outputs.

However, despite these daily-scale uncertainties, the GCM ensemble demonstrates a strong ability to represent the local climatology after bias correction. The comparison of climatological normals (Figure 4) reveals a good agreement between the model-simulated and observed monthly precipitation averages, successfully capturing the basin's seasonal patterns. This agreement at a climatological scale provides confidence that the models are suitable for their intended purpose: assessing long-term changes in hydrological responses under future scenarios (Oliveira et al. 2023; Almazroui et al. 2021; Medeiros et al. 2022). Nevertheless, we acknowledge that this input uncertainty propagates through the hydrological model, and thus the streamflow projections should be interpreted as representing a range of potential future trends rather than as exact forecasts. A key finding is the projected increase in streamflow peaks, with values exceeding 1000 m^3/s in the MRR under the high-emission scenario. This occurs despite a projected decline in total annual rainfall, a paradox explained by the changing nature of precipitation. As introduced earlier, future climate scenarios suggest rainfall will become more concentrated in shorter, more intense events (Almazroui et al. 2021; Jiménez-Navarro et al. 2021). This high-intensity precipitation exceeds the soil's infiltration capacity, leading to a higher percentage of surface runoff and, consequently, more extreme flood peaks.

A significant limitation in the hydrological modelling concerns the SWAT model's performance at the Toritama station, which was deemed unsatisfactory during the validation period (NSE = 0.41). This statistical result is visually confirmed in Figure S1, which shows discrepancies where the model over- and underestimates peak flows.

This poor performance is strongly attributed to the unquantified influence of upstream reservoirs (Andrade et al. 2021; Siqueira et al. 2021; de Farias et al. 2024), particularly, the Poço Fundo and Engenheiro Gercino Pontes reservoirs. These structures heavily regulate the river's natural flow regime by storing water during wet periods and releasing it during dry periods to meet water supply demands. As daily operational data—such as release schedules and storage volumes—were unavailable for this study, the SWAT model cannot accurately simulate these artificial alterations to the streamflow. This lack of management data is a primary source of error, especially during the validation period where reservoir operations may have significantly differed from the calibration period.

Future research in this basin would therefore substantially benefit from the inclusion of such reservoir management data. Incorporating daily release information into the SWAT model would likely lead to a significant improvement in performance at the Toritama station. Alternatively, employing a modelling approach that explicitly integrates reservoir operation modules could also provide a more accurate representation of the basin's hydrology. Consequently, while the model's performance is satisfactory at downstream stations, the projections for the upper portion of the basin should be interpreted with additional caution due to this specific limitation.

A further source of uncertainty arises from the land use change modelling. The validation of the LCM indicated that the 'Agriculture' class had the lowest modelling accuracy, with an unsatisfactory KIA of 0.4121 (Table S6). This is a notable concern, as the transition probability matrix showed 'Agriculture' to be a highly dynamic class, with approximately 27.01% of its area tending to be converted to 'Pasture' over the analysed period (Table S5).

As the 'Agriculture' and 'Pasture' classes are assigned distinct hydrological parameters within the SWAT model, which influence variables such as surface runoff and evapotranspiration, the low accuracy in spatially predicting these transitions inevitably propagates uncertainty into the simulated water balance components. This, in turn, affects the final streamflow projections. This limitation adds another layer of uncertainty to the study's findings, reinforcing that the projections should be interpreted as plausible future trends rather than precise forecasts.

5 | Conclusions

This study addressed key questions on the hydrological response of a transitional basin spanning semiarid and humid tropical forest biomes under coupled climate and land cover change. Our findings reveal that this complex ecotone is, particularly, vulnerable to climate change, especially under high-emission scenarios (SSP5–8.5). A key hydrological process identified is the paradoxical shift in streamflow behaviour: despite projections of declining total rainfall, the simulations show that rising temperatures and altered precipitation patterns could result in an intensification of streamflow extremes, posing challenges to future water availability. These changes underscore the critical need for adaptive water management strategies tailored to regional conditions, particularly, in areas experiencing both urban expansion and agricultural pressure.

The study identified significant land use and land cover transformations, such as the conversion of native vegetation into pasture and agricultural areas, particularly, in the Caatinga–Atlantic Forest transition zone. These changes directly impact the basin's water balance, demonstrating a clear differential mediation of hydrological processes by land cover type. Analysing these variables by land use and land cover class revealed that urban areas are more susceptible to surface runoff due to soil impermeability, increasing the risk of flooding, particularly, during intense rainfall events predicted by future scenarios. Pasture and agricultural areas also show significant variations in surface runoff, reflecting moderate vulnerability to change. While agricultural areas may facilitate infiltration, intensive farming practices contribute to increased runoff, a pattern also observed in pasture areas. Soil compaction and rainfall conditions similarly affect both land use and land cover classes. Native vegetation areas exhibited low runoff levels, with a greater capacity for water infiltration.

Precipitation projections suggest higher variability during wetter months and lower variability during drier months. This indicates potentially greater stability in dry season conditions but increased flood risk during the rainy season. Coastal and highly urbanised regions, such as the Recife Metropolitan Region (MRR), appear more exposed to extreme events, with higher flow peaks, whereas more inland regions (UA1 and UA4) exhibit smaller variations in hydrological regimes, even under more extreme scenarios. Although the projections indicate significant hydrological changes, it is crucial to recognise that model uncertainties remain considerable, particularly, in precipitation estimates. This underscores the importance of considering multiple models and scenarios to reduce projection uncertainties. Consequently, the results should be interpreted as potential future trends rather than precise forecasts.

To translate these findings into actionable adaptive strategies, we offer specific policy recommendations. For instance, the projection of streamflow peaks exceeding 1000 m^3/s in the MRR under a high-emission, long-term scenario highlights the urgent need for investments in urban flood control. This includes both structural measures, such as enhancing pluvial drainage systems and constructing retention reservoirs, and non-structural measures, like updating urban planning to restrict soil impermeabilization in vulnerable areas. Furthermore, our results show a clear hydrological distinction between biomes, with the Atlantic Forest exhibiting a high capacity for groundwater recharge compared to the lower recharge capacity observed in the Caatinga. This underscores the importance of biome-specific conservation policies, such as implementing Payment for Environmental Services (PES) to protect the remaining Atlantic Forest fragments, thereby safeguarding critical water recharge zones. For the Caatinga, policies should encourage soil management and adapted agricultural techniques that improve water retention and resilience to drought.

The study highlights the need for adaptive strategies in the management of the basin's water resources to mitigate the adverse effects of climate change, ensuring the sustainability of water resources and the preservation of ecosystems in the Capibaribe River basin. It also emphasises that for a region as crucial as Pernambuco, public policies focused on climate change adaptation and proper natural resource management are essential.

Acknowledgements

The authors would like to thank the Foundation for the Support of Science and Technology of the State of Pernambuco (FACEPE) for its research support and the provision of a postgraduate scholarship, and the Coordination for the Improvement of Higher Education Personnel (CAPES) for the financial support granted through the Sandwich PhD scholarship, linked to the Institutional Internationalisation Program (PRINT) of the first author. The Article Processing Charge for the publication of this research was funded by the Coordenação de Aperfeiçoamento de Pessoal de Nível Superior - Brasil (CAPES) (ROR identifier: 00x0ma614).

Ethics Statement

The authors have nothing to report.

Consent

The authors have nothing to report.

Data Availability Statement

Bias-corrected dataset: https://doi.org/10.57760/sciencedb.02316; Observed rainfall: http://www.snirh.gov.br/hidroweb; Observed runoff: http://www.snirh.gov.br/hidroweb; Meteorological data: https://portal.inmet.gov.br/dadoshistoricos; Digital elevation model: https://earthdata.nasa.gov; Soil map: https://geoinfo.dados.embrapa.br/catalogue/#/dataset/2993; Soil physical-hydrological characteristics: https://www.sisolos.cnptia.embrapa.br; Land use and land cover: https://brasil.mapbiomas.org/colecoes-mapbiomas/.

References

Abbas, S. A., Y. Xuan, A. H. Al-Rammahi, and H. F. Addab. 2022. "A Comparison Study of Observed and the CMIP5 Modelled Precipitation Over Iraq 1941–2005." *Atmosphere* 13: 1869. https://doi.org/10.3390/atmos13111869.

Abbaspour, K. C. 2011. *SWAT-CUP2009: SWAT Calibration and Uncertainty Programs—A User Manual*, 95. Department of Systems Analysis, Integrated Assessment and Modelling (SIAM), 112 Eawag, Swiss Federal Institute of Aquatic Science and Technology.

Abbaspour, K. C. 2015. *SWAT-CUP2012: SWAT Calibration and Uncertainty Programs—A User Manual*, 100. Department of Systems Analysis, Integrated Assessment and Modelling (SIAM), Eawag, Swiss Federal Institute of Aquatic Science and Technology.

Aguiar, J. L., L. P. Diniz, and M. Melo Júnior. 2024. "Dryland Reservoirs Support Greater Taxonomic and Functional Beta Diversity of Zooplankton Regardless of Hydrological Period." *Hydrobiologia* 851: 4019–4031. https://doi.org/10.1007/s10750-024-05558-7.

Almagro, A., P. T. S. Oliveira, M. A. Nearing, and S. Hagemann. 2017. "Projected Climate Change Impacts in Rainfall Erosivity Over Brazil." *Scientific Reports* 7: 8130. https://doi.org/10.1038/s41598-017-08298-y.

Almazroui, M., M. Ashfaq, M. N. Islam, et al. 2021. "Assessment of CMIP6 Performance and Projected Temperature and Precipitation Changes Over South America." *Earth Systems and Environment* 5, no. 2: 155–183. https://doi.org/10.1007/s41748-021-00233-6.

Alves, R. N., C. F. Mariz Jr., M. K. de Melo Alves, et al. 2021. "Contamination and Toxicity of Surface Waters Along Rural and Urban Regions of the Capibaribe River in Tropical Northeastern Brazil." *Environmental Toxicology and Chemistry* 40, no. 11: 3063–3077.

Andrade, C. W. L., S. M. G. L. Montenegro, A. A. A. Montenegro, J. R. Lima, R. Srinivasan, and C. A. Jones. 2021. "Climate Change Impact Assessment on Water Resources Under RCP Scenarios: A Case Study in Mundaú River Basin, Northeastern Brazil." *International Journal of Climatology* 41, no. Suppl. 1: E1045–E1061. https://doi.org/10.1002/joc.6751.

Anil, S., and P. A. Raj. 2022. "Deciphering the Projected Changes in CMIP-6 Based Precipitation Simulations Over the Krishna River Basin." *Journal of Water and Climate Change* 13, no. 3: 1389. https://doi.org/10.2166/wcc.2022.399.

Araujo, D. C. d. S., S. M. G. L. Montenegro, S. F. Silva, V. E. M. de Farias, and A. B. Rodrigues. 2024. "Analysis of Climate Change Scenarios Using CMIP6 Models in Pernambuco, Brazil." *Revista Brasileira de Ciências Ambientais* 59: e1868. https://doi.org/10.5327/Z2176-94781868.

Arnold, J. G., D. N. Moriasi, P. W. Gassman, et al. 2012. "SWAT: Model Use, Calibration, and Validation." *American Society of Agricultural and Biological Engineers, Transactions of the ASABE* 55, no. 4: 1491–1508.

Arnold, J. G., R. Srinivasan, R. S. Muttiah, and J. Williams. 1998. "Large Area Hydrologic Modeling and Assessment: Part I - Model Development." *Journal of the American Water Resources Association* 34, no. 1: 73–90. https://doi.org/10.1111/j.1752-1688.1998.tb05961.x.

Ashu, A. B., and S. I. Lee. 2023. "Multi-Site Calibration of Hydrological Model and Spatio-Temporal Assessment of Water Balance in a Monsoon Watershed." *Water* 15: 360. https://doi.org/10.3390/w15020360.

Ballarin, A. S., J. S. Sone, G. C. Gesualdo, et al. 2023. "CLIMBra—Climate Change Dataset for Brazil." *Scientific Data* 10: 1–31. https://doi.org/10.1038/s41597-023-01956-z.

Clark Labs. 2020. "Land Change Modeller (LCM)." In *TerrSet. Geospatial Monitoring System*, edited by J. R. Eastman, 206–219. Clark University.

Da Silva, P. E., C. M. Santos e Silva, M. H. C. Spyrides, and A. L. M. Barbosa. 2019. "Precipitation and Air Temperature Extremes in the Amazon and Northeast Brazil." *International Journal of Climatology* 39: 579–595. https://doi.org/10.1002/joc.5829.

da Silva, Y. J. A. B., J. R. B. Cantalice, V. P. Singh, C. M. C. A. Cruz, and W. L. S. Souza. 2016. "Sediment Transport Under the Presence and Absence of Emergent Vegetation in a Natural Alluvial Channel From Brazil." *International Journal of Sediment Research* 31, no. 4: 360–367. https://doi.org/10.1016/j.ijsrc.2016.01.001.

de Andrade Costa, D., Y. Bayissa, M. D. Villas-Boas, et al. 2024. "Water Availability and Extreme Events Under Climate Change Scenarios in an Experimental Watershed of the Brazilian Atlantic Forest." *Science of the Total Environment* 946: 174417. https://doi.org/10.1016/j.scitotenv.2024.174417.

de Arruda Gomes, M. M., L. F. de Melo Verçosa, and J. A. Cirilo. 2021. "Hydrologic Models Coupled With 2D Hydrodynamic Model for High-Resolution Urban Flood Simulation." *Natural Hazards* 108: 3121–3157. https://doi.org/10.1007/s11069-021-04817-3.

de Farias, V. E. M., A. B. Rodrigues, P. B. C. L. Monteiro, D. C. S. Araujo, S. M. G. L. Montenegro, and J. J. S. P. Cabral. 2024. "Perspectivas climáticas futuras com base nos modelos do CMIP para municípios da Região Metropolitana do Recife (PE), Brasil." *Caminhos de Geografia* 25: 58–79. https://doi.org/10.14393/RCG2510171642.

Diaz, C. C. F. 2021. Impactos da dinâmica de uso e cobertura da terra sobre os recursos hídricos da bacia hidrográfica do rio Capibaribe. 134 f. Tese (Doutorado) - Universidade Federal de Pernambuco, CFCH. Programa de Pós-graduação em Geografia, Recife.

EMBRAPA—Empresa Brasileira de Agropecuária. 2018. *Sistema Brasileiro de Classificação dos Solos*. 5th ed, 356. Embrapa.

Fernandes, J. G., R. C. A. P. Galindo, A. L. D. Bocage Neta, C. A. Jones, and R. Srinivasan. 2020. "Systematization of Vegetation Data for the Caatinga Biome for SWAT Hydrological Basin Modeling." *Pesquisa Agropecuária Pernambucana* 24, no. 2. https://doi.org/10.12661/pap.2019.008.

Ferreira, T. S. G. 2020. "Análise de desempenho do modelo SWAT para a bacia do Rio Capibaribe e estimativa do aporte de sedimentos a seus reservatórios." Dissertação (Mestrado)—Universidade Federal de Pernambuco, CAA, Engenharia Civil e Ambiental, 145.

Frade, T. G., C. A. G. Santos, and R. M. Silva. 2024. "Simulating Future Hydrological Droughts and Sediment Yield by Integrating Different Climate Scenarios for a Semiarid Basin in Brazil." *Stochastic Environmental Research and Risk Assessment* 38: 985. https://doi.org/10.1007/s00477-024-02777-1.

Hamdy, O., S. Zhao, M. A. Salheen, and Y. Y. Eid. 2017. "Analyses the Driving Forces for Urban Growth by Using IDRISI Selva Models Abouelreesh e Aswan as a Case Study." *International Journal of Engineering and Technology* 9, no. 3: 226–232. https://doi.org/10.7763/ijet.2017.v9.975.

Heo, J.-H., H. Ahn, J.-Y. Shin, T. R. Kjeldsen, and C. Jeong. 2019. "Probability Distributions for a Quantile Mapping Technique for a Bias Correction of Precipitation Data: A Case Study to Precipitation Data Under Climate Change." *Water (Basel)* 11, no. 7: 1475. https://doi.org/10.3390/w11071475.

IPCC (Intergovernmental Panel on Climate Change). 2023. "Oceans and Coastal Ecosystems and Their Services." In *Climate Change 2022 – Impacts, Adaptation and Vulnerability: Working Group II Contribution to the Sixth Assessment Report of the Intergovernmental Panel on Climate Change*, 379–550. Cambridge University Press.

Jiménez-Navarro, I. C., P. Jimeno-Sáez, A. López-Ballesteros, J. Pérez-Sánchez, and J. Senent-Aparicio. 2021. "Impact of Climate Change on the Hydrology of the ForestedWatershed That Drains to Lake Erken in Sweden: An Analysis Using SWAT+ and CMIP6 Scenarios." *Forests* 12: 1803. https://doi.org/10.3390/f12121803.

Leão, E. B. S., J. C. S. Andrade, and L. F. Nascimento. 2021. "Recife: A Climate Action Profile." *Cities* 116: 103270. https://doi.org/10.1016/j.cities.2021.103270.

Lima, M. C. G., S. M. F. Sá, W. M. Souza, and T. E. M. Santos. 2018. "Generated Impacts and the Management of the Capibaribe River

Basin-PE." *Journal of Environmental Analysis and Progress* 3: 75–85. https://doi.org/10.24221/jeap.3.1.2018.1658.075-085.

Medeiros, F. J., C. P. Oliveira, and A. Avila-Diaz. 2022. "Evaluation of Extreme Precipitation Climate Indices and Their Projected Changes for Brazil: From CMIP3 to CMIP6." *Weather and Climate Extremes* 38: 100511. https://doi.org/10.1016/j.wace.2022.100511.

Mishra, V. N., P. K. Rai, and K. Mohan. 2014. "Prediction of Land Use Changes Based on Land Change Modeler (LCM) Using Remote Sensing: A Case Study of Muzaffarpur (Bihar), India." *Journal of the Geographical Institute Jovan Cvijic SASA* 64, no. 1: 111–127. https://doi.org/10.2298/IJGI1401111M.

Moriasi, D. N., M. W. Gitau, N. Pai, and P. Daggupati. 2015. "Hydrologic and Water Quality Models: Performance Measures and Evaluation Criteria." *Transactions of the ASABE* 58, no. 6: 1763–1785. https://doi.org/10.13031/trans.58.10715.

Oliveira, D. M., J. G. M. Ribeiro, L. F. Faria, and M. S. Reboita. 2023. "Performance dos modelos climáticos do CMIP6 em simular a precipitação em subdomínios da América do Sul no período histórico." *Revista Brasileira de Geografia Física* 16, no. 1: 116–133.

Preis, C. M., D. Franco, and S. C. Varela. 2021. "Avaliação do uso e ocupação do solo na bacia hidrográfica do rio Itajaí e simulação para 2027." *São Paulo, UNESP, Geociências* 40, no. 2: 407–414. https://doi.org/10.5016/geociencias.v40i02.14321.

Ribeiro Neto, A., C. A. Scott, E. A. Lima, S. M. G. L. Montenegro, and J. A. Cirilo. 2014. "Infrastructure Sufficiency in Meeting Water Demand Under Climate-Induced Sociohydrological Transition in the Urbanizing Capibaribe River Basin-Brazil." *Hydrology and Earth System Sciences* 18: 3449–3459. https://doi.org/10.5194/hess-18-3449-2014.

Rocha, P. I. O., A. P. X. Dantas, R. M. Silva, and C. A. G. Santos. 2024. "Modeling Urban Forest Loss and Future Urban Expansion as Support for Planning and Territorial Organization in João Pessoa City, Brazil." *Modeling Earth Systems and Environment* 10: 256. https://doi.org/10.1007/s40808-024-01983-8.

Sadhwani, K., T. I. Eldho, M. K. Jha, and S. Karmakar. 2022. "Effects of Dynamic Land Use/Land Cover Change on Flow and Sediment Yield in a Monsoon-Dominated Tropical Watershed." *Water* 14: 3666. https://doi.org/10.3390/w14223666.

Santos, J. Y. G., S. M. G. L. Montenegro, R. M. Silva, et al. 2021. "Modeling the Impacts of Future LULC and Climate Change on Runoff and Sediment Yield in a Strategic Basin in the Caatinga/Atlantic Forest Ecotone of Brazil." *Catena* 203: 105308. https://doi.org/10.1016/j.catena.2021.105308.

Shrestha, M., S. C. Acharyaa, and P. K. Shrestha. 2017. "Bias Correction of Climate Models for Hydrological Modelling—Are Simple Methods Still Useful?" *Meteorological Applications* 24: 531–539. https://doi.org/10.1002/met.1655.

Silva, A. M., R. M. Silva, C. A. G. Santos, F. M. Linhares, and A. P. C. Xavier. 2022. "Modeling the Effects of Future Climate and Land Use Changes on Streamflow in a Headwater Basin in the Brazilian Caatinga Biome." *Geocarto International* 37: 12436–12465. https://doi.org/10.1080/10106049.2022.2068672.

Silva, D. J. F., T. R. F. Silva, M. L. Oliveira, et al. 2024. "Analysis of Surface Radiation Fluxes and Environmental Variables Over Caatinga Vegetation With Different Densities." *Journal of Arid Environments* 222: 105163. https://doi.org/10.1016/j.jaridenv.2024.105163.

Silva, F. B. R., J. C. P. dos Santos, A. B. da Silva, et al. 2001. *Zoneamento Agroecológico do Estado de Pernambuco—ZAPE*. Embrapa Solos – Unidade de Execução de Pesquisa e Desenvolvimento – UEP/Recife. https://geoinfo.dados.embrapa.br/catalogue/#/dataset/2993.

Silva, L. P., A. P. C. Xavier, R. M. Silva, and C. A. G. Santos. 2020. "Modeling Land Cover Change Based on an Artificial Neural Network for a Semiarid River Basin in Northeastern Brazil." *Global Ecology and Conservation* 21: e00811. https://doi.org/10.1016/j.gecco.2019.e00811.

Siqueira, P., P. Oliveira, D. Bressiani, A. A. Meira Neto, and D. B. Rodrigues. 2021. "Effects of Climate and Land Cover Changes on Water Availability in a Brazilian Cerrado Basin." *Journal of Hydrology: Regional Studies* 37: 100931. https://doi.org/10.1016/j.ejrh.2021.100931.

Song, Y. H., M. S. Nashwan, E. S. Chung, and S. Shahid. 2021. "Advances in CMIP6 INM-CM5 Over CMIP5 INM-CM4 for Precipitation Simulation in South Korea." *Atmospheric Research* 247: 105261. https://doi.org/10.1016/j.atmosres.2020.105261.

Takele, G. S., G. S. Gebrie, A. G. Gebremariam, and A. N. Engida. 2022. "Future Climate Change and Impacts on Water Resources in the Upper Blue Nile Basin." *Journal of Water and Climate Change* 13, no. 2: 908–925. https://doi.org/10.2166/wcc.2021.235.

Tan, M. L., J. Liang, N. Samat, N. W. Chan, J. M. Haywood, and K. Hodges. 2021. "Hydrological Extremes and Responses to Climate Change in the Kelantan River Basin, Malaysia, Based on the CMIP6 HighResMIP Experiments." *Water* 13: 1472. https://doi.org/10.3390/w13111472.

Tenagashaw, D. Y., M. Muluneh, G. Metaferia, and Y. A. Mekonnen. 2022. "Land Use and Climate Change Impacts on Streamflow Using SWAT Model, Middle Awash Sub Basin, Ethiopia." *Water Conservation Science and Engineering* 7: 183–196. https://doi.org/10.1007/s41101-022-00135-2.

Todaro, V., M. D'Oria, D. Secci, A. Zanini, and M. G. Tanda. 2022. "Climate Change Over the Mediterranean Region: Local Temperature and Precipitation Variations at Five Pilot Sites." *Water* 14: 2499. https://doi.org/10.3390/w14162499.

Wang, X., J. Yang, J. Xiong, et al. 2022. "Investigating the Impact of the Spatiotemporal Bias Correction of Precipitation in CMIP6 Climate Models on Drought Assessments." *Remote Sensing* 14: 6172. https://doi.org/10.3390/rs14236172.

Wen, K., B. Gao, and M. Li. 2021. "Quantifying the Impact of Future Climate Change on Runoff in the Amur River Basin Using a Distributed Hydrological Model and CMIP6 GCM Projections." *Atmosphere* 12: 1560. https://doi.org/10.3390/atmos12121560.

Xavier, A. C., C. W. King, and B. R. Scanlon. 2016. "Daily Gridded Meteorological Variables in Brazil (1980–2013)." *International Journal of Climatology* 36: 2644–2659. https://doi.org/10.1002/joc.4518.

Xavier, A. P. C., and R. M. Silva. 2018. "A GIS-Based Method for Temporal Dynamic Modelling of the Land Use and Land Cover in the Tapacurá River Basin (PE)." *Geociências* 37, no. 1: 193–210. https://doi.org/10.5016/geociencias.v37i1.12623.

Xue, P., C. Zhang, Z. Wen, F. Park, and H. Jakada. 2022. "Climate Variability Impacts on Runoff Projection Under Quantile Mapping Bias Correction in the Support CMIP6: An Investigation in Lushi Basin of China." *Journal of Hydrology* 614: 128550. https://doi.org/10.1016/j.jhydrol.2022.128550.

Supporting Information

Additional supporting information can be found online in the Supporting Information section. **Figure S1:** Hydrograph of observed and calibrated discharges and hyetograph of mean monthly precipitation for each gauging station within the Capibaribe River basin. **Table S1:** Global climate models used in this study, adapted from Ballarin et al. (2023). **Table S2:** Explanatory variables tested in the dynamics of land use and land cover. **Table S3:** Rainfall, climate and streamflow stations within the Capibaribe River basin. **Table S4:**. Classification of modelling efficiency, adapted from Moriasi et al. (2015). **Table S5:** Probability matrix of land use and land cover change between 2010 and 2020. **Table S6:** Agreement level between simulated t_3 in the LCM and observed t_3 for the basin. **Table S7:** Statistical performance of precipitation from each climate model compared to the mean of 10 climate models under scenarios SSP2–4.5 (C1) and SSP5–8.5 (C2).